UNIVERSITY OF TURKU

Phenotypic characterization of hypertrophic cardiomyopathy in human iPSC-derived heart organoids carrying a *JPH2* variant

Physiology and Genetics
Department of Biology
Master's thesis

Author:
Anni Marjomaa

18.5.2026
Turku

Master's thesis

Subject: Biology, Physiology and Genetics
Author: Anni Marjomaa
Title: Phenotypic characterization of hypertrophic cardiomyopathy in human iPSC-derived heart organoids carrying a *JPH2* variant
Supervisors: Martta Häkli, Katriina Aalto-Setälä, Heidi Viitaniemi
Number of pages: 59 pages
Date: 18.5.2026

Hypertrophic cardiomyopathy (HCM) is a hereditary cardiac disease characterized by abnormal thickening of the left ventricular wall, due to cardiomyocyte hypertrophy and myocardial fibrosis, leading to altered cardiac function and increased risk of arrhythmias. HCM is estimated to occur in one in 500 people and is a leading cause of sudden cardiac death in young people, particularly athletes. Despite its clinical importance, understanding the molecular and cellular mechanisms of HCM remains limited, due to the lack of physiologically relevant disease models. Current *in vitro* models, mainly 2D cultures of human induced pluripotent stem cell (hiPSC)-derived cardiomyocytes fail to recapitulate the multicellular interactions contributing to disease progression, highlighting the need for more advanced HCM models.

This master's thesis focused on generation of 3D heart organoids carrying a *JPH2* variant and their use in the phenotypic characterization of HCM to improve *in vitro* disease modeling. Heart organoids were generated from patient-derived hiPSCs carrying a *JPH2* (Thr161Lys) variant using a self-assembly method. Phenotypic characterization included immunocytochemistry, functional analysis and gene expression analysis.

Heart organoid generation was optimized, resulting in successful generation of heart organoids, with multiple cardiac cell types, including cardiomyocytes, cardiac fibroblasts, and smooth muscle cells. However, transcriptional analysis did not reveal clear differences between HCM and control organoids. Instead, gene expression patterns were primarily influenced by time point and culture medium. Additionally, medium affected the contractile behavior of spontaneously beating organoids. In conclusion, the HCM phenotype was not yet evident in heart organoids and further optimization is required.

Key words: hypertrophic cardiomyopathy, JPH2, disease modeling, heart organoids, hiPSCs.

Pro gradu -tutkielma

Pääaine: Biologia, Fysiologian ja Genetiikan linja
Tekijä: Anni Marjomaa
Otsikko: Phenotypic characterization of hypertrophic cardiomyopathy in human iPSC-derived heart organoids carrying a *JPH2* variant
Ohjaajat: Martta Häkli, Katriina Aalto-Setälä, Heidi Viitaniemi
Sivumäärä: 59 sivua
Päivämäärä: 18.5.2026

Hypertrofinen kardiomyopatia (HCM) on perinnöllinen sydänsairaus, jossa sydänlihas paksuuntuu erityisesti vasemman kammion alueella. Tämä johtuu pääasiassa sydänlihassolujen hypertrofiasta ja sydänlihaskudoksessa esiintyvästä fibroosista, mitkä yhdessä heikentävät sydämen toimintaa ja lisäävät rytmihäiriöiden riskiä. HCM:n esiintyvyydeksi arvioidaan noin yksi tapaus 500 henkilöä kohden, se on yleisin sydänperäisen äkkikuoleman syy nuorilla ja urheilijoilla. Taudin kliinisestä merkityksestä huolimatta sen molekyylitason ja solutason mekanismit tunnetaan vain osittain, fysiologisesti relevanttien tautimallien puutteen vuoksi. Nykyiset *in vitro* -menetelmät, kuten 2D ihmisen indusoiduista pluripotenteista kantasoluista (hiPSC) erilaistetut sydänlihassoluviljelmät eivät kykene mallintamaan taudin etenemiseen vaikuttavia monisoluisia vuorovaikutuksia. Tämä korostaa tarvetta kehittyneemmille tautimalleille.

Tämän pro gradu -tutkielman tavoitteena oli kehittää 3D-sydänorganoidimalli HCM:n tutkimiseen, joka mahdollistaisi taudin tarkemman mallintamisen verrattuna nykyisiin *in vitro* -malleihin. Sydänorganoidit tuotettiin potilasperäisistä hiPSC-soluista, jotka kantoivat JPH2 (Thr161Lys) varianttia, hyödyntäen solujen itseorganisoitumiseen perustuvaa menetelmää. Sydänorganoidien fenotyyppinen karakterisointi sisälsi immunosytokemiaa, toiminnallisia analyysejä ja geenienekspressiotutkimuksia.

Sydänorganoidien menetelmää optimoitiin, ja onnistuneesti tuotetut organoidit sisälsivät sydänlihassoluja ja muita sydämessä esiintyviä solutyyppejä, kuten fibroblasteja ja sileälihassoluja. Transkriptiotason analyysissä ei kuitenkaan havaittu selkeitä eroja HCM- ja kontrolliorganoidien välillä, vaan geenieksprессioon vaikuttivat pääasiassa aikapiste ja käytetty viljelymedium. Viljelymedium vaikutti myös spontaanisti sykkivien organoidien supistuvuuteen. Tämän tutkielman perusteella HCM-fenotyypin ilmentyminen ei ollut vielä selkeästi havaittavissa, mikä korostaa sydänorganoidimallin jatkokehityksen ja optimoinnin merkitystä.

Avainsanat: hypertrofinen kardiomyopatia, JPH2, tautimallinnus, sydänorganoidit, hiPSCs

Table of contents

1 Introduction

1.1 The heart

1.1.1 Cardiovascular system

The cardiovascular system comprises the heart, blood vessels, and lymphatic vessels, and its main function is to transport blood and lymph to and from the tissues of the body (Pawlina 2024). The heart has an essential role as a muscular pump that drives blood circulation through the vascular network, ensuring the delivery of oxygen and nutrient to tissues, the distribution of hormones, and immune cells, and the removal of carbon dioxide and metabolic waste (Shah et al. 2022; Pawlina 2024; Gray 2025). Arterial blood is pumped under high pressure through arteries that deliver blood to a network of narrow, thin-walled capillaries, where the exchange of gases, nutrients, and waste between blood and tissues occurs (Pawlina 2024). After the exchange, venous blood is returned to the heart through veins under low pressure. Overall, the heart supports two circulations: pulmonary circulation, in which the right side of the heart pumps blood to the lungs and back, and systemic circulation, in which the left side pumps blood through aorta to the rest of the body and back (Pawlina 2024).

To support this circulatory function, human heart has a highly specialized anatomical organization consisting of four chambers that are distinct both morphologically and functionally: right atrium, right ventricle, left atrium and left ventricle (Figure 1) (Litviňuková et al. 2020). The atria receive venous blood, function as reservoirs and facilitate ventricular filling. Ventricles then generate the powerful contractions required to propel blood into the main arteries (Gray 2025). Deoxygenated blood from the low-pressure right atrium and ventricle is bumped through pulmonary arteries to the lungs for oxygenation (Pawlina 2024). The left atrium receives oxygenated blood via pulmonary veins, which is then pumped through left ventricle for systemic distribution at high pressure. Blood is pumped from the ventricles during systole, the contraction phase of the cardiac cycle, whereas during diastole the ventricles relax and fill with blood (Pawlina 2024). The cardiac chambers are separated by interatrial and interventricular septum, and atrio-ventricular and ventricular-arterial valves maintain unidirectional blood flow (Litviňuková et al. 2020; Pawlina 2024).

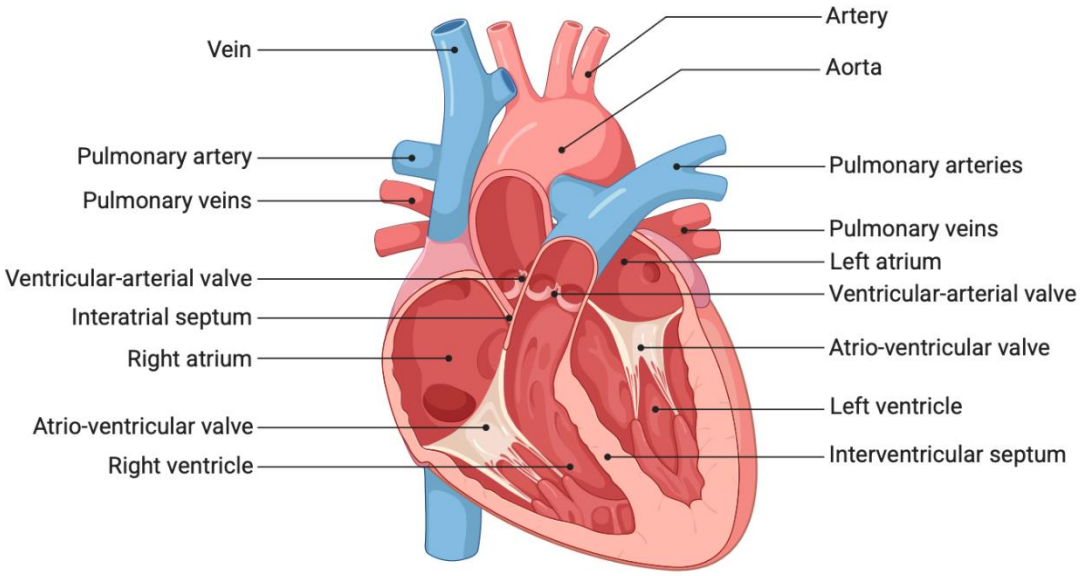

Figure 1. Schematic overview of heart anatomy. Created in BioRender.com (adapted from a template by Jean-Francis Berry & Sally Kim).

The heart is located in the thoracic cavity and is surrounded by pericardium. Furthermore, the heart wall is organized into three layers: epicardium on the outside, myocardium in the middle, and endocardium lining the inner chamber surfaces (Pawlina 2024). The epicardium is a protective mesothelial layer surrounding the heart that persists from early development into adulthood (Fernandes et al. 2023). Myocardium comprises of cardiac muscle and forms the main structural component of the heart (Pawlina 2024). The thickness of the myocardium varies depending on the location of the heart, being thinner in the atria than in the ventricles as well as being thinner in the right ventricle than in the left ventricle. These differences reflect variation in the pressures required to pump blood in pulmonary and systemic circulations (Pawlina 2024).

Beyond its structural organization, the heart depends on a specialized electrical conducting system to coordinate contraction of its chambers independently. This conduction system consists of specialized cardiomyocytes (CMs) (Padala et al. 2020). Electrical impulses needed for contraction originate in the sinoatrial node, travel through the atrioventricular (AV) node, continue along the AV bundle that divides into two, right and left branches, going into both ventricles. In the ventricles, Purkinje fibers distribute the electrical stimulus to the myocardium, coordinating ventricular contraction (Litviňuková et al. 2020; Pawlina 2024).

The structural and functional complexity of the heart relies on tightly coordinated interactions among diverse cardiac cell types, enabling continuous contraction and relaxation under

location-specific mechanical and hemodynamic demands (Litviňuková et al. 2020). CMs are responsible for the contractile function of the heart (Harvey & Leinwand 2011). CMs also represent the most abundant cardiac cell type and can be classified into atrial and ventricular CMs, with ventricular CMs comprising the majority present in the ventricles (Litviňuková et al. 2020). At the cellular level, in addition to CMs, the human heart contains several other cell types, including cardiac fibroblasts (cFBs), smooth muscle cells (SMCs), and endothelial cells (ECs), under neurohormonal control (Mosqueira et al. 2019). Furthermore, other cell types present in the adult human heart include adipocytes, pericytes, mesothelial cells and immune cells (Litviňuková et al. 2020).

In addition to diverse cardiac cell types, cardiac tissue is supported by the extracellular matrix (ECM), which contributes to both structural support and regulation of cardiac function (Park et al. 2021). More precisely, ECM is cell-free three-dimensional (3D) network of proteins and proteases that forms a fibrillar scaffold in which cardiac cells are embedded. In the myocardium, major ECM components include collagen, elastin, fibronectin, laminin, glycosaminoglycans, and proteoglycans, with collagen being the most abundant. Furthermore, the ECM is dynamically regulated and can undergo remodeling in response to cellular demand or injury, as well as support cardiac development. Therefore, ECM affects also cardiac cellular behavior through mechanical and biochemical signaling. In particular, cFBs have a central role in maintaining and remodeling ECM by regulating the synthesis and degradation of ECM components, while ECM in turn regulates fibroblast activity. This bidirectional interaction between the cardiac cells and ECM modulates fundamental cellular processes such as survival, proliferation, migration, and differentiation (Park et al. 2021).

To result in such structural and functional complexity, cardiac development is a tightly regulated process both spatially and temporally (Tian et al. 2010). Cardiac development begins early in embryogenesis when the heart is among the first organs to form (Horitani & Shiojima 2024). During this period, Wnt signaling plays an essential role in the early specification and differentiation of cardiac progenitor cells. More specifically, Wnt signaling guides mesodermal cells toward the cardiac lineage and thereby initiates heart development. Early activation of Wnt signaling promotes early cardiac specification, whereas later activation suppresses cardiomyocyte differentiation, highlighting the pathway's temporal and spatial role in cardiac development (Horitani & Shiojima 2024).

1.1.2 Cardiac excitation-contraction coupling

Contraction of cardiac muscle results from a cascade of signaling events (Landstrom et al. 2011). This process, known as cardiac excitation-contraction coupling (ECC), enables electrical excitation (action potentials) at the cell membrane to be converted into mechanical contraction in CMs (Beavers et al. 2014). Notably, calcium plays a major role in cardiac contraction, which is regulated by changes in intracellular calcium (Ca^{2+}) concentration (Eisner et al. 2017). Proper cardiac function requires that intracellular Ca^{2+} levels increase during systole to enable ventricular contraction and pumping of blood and subsequently decrease rapidly to low enough levels during diastole to allow myocardial relaxation and ventricular filling. A large proportion of Ca^{2+} required for contraction is stored in the sarcoplasmic reticulum (SR) and released through calcium-induced calcium release (CICR). This tightly regulated control of intracellular Ca^{2+} is orchestrated by various ion channels, transporters, and pumps that are precisely organized within CMs (Eisner et al. 2017).

When the action potential reaches the CMs, the signaling cascade is activated. On the CM plasma membrane (PM) and transverse tubules (t-tubules), membrane depolarization opens L-type Ca^{2+} channels (LTCCs), facilitating the influx of extracellular Ca^{2+} (Landstrom et al. 2011). This increase of intracellular Ca^{2+} triggers further Ca^{2+} release from the SR through ryanodine receptor 2 (RyR2) channels in CICR, leading to substantial increase in intracellular Ca^{2+} levels. After this, CM relaxation occurs as intracellular Ca^{2+} is removed from the cytoplasm primarily by uptake back into the SR through SR Ca^{2+} ATPase (SERCA) with the help of phospholamban (PLB), or by transporting it out of the cell through sodium-calcium exchanger (NCX) (Landstrom et al. 2011; Eisner et al. 2017).

In addition to coordinated signaling events, CMs rely on highly organized cellular architecture to maintain efficient ECC. A key component of this organization is formed by junctional membrane complexes (JMCs), which connect the t-tubule membrane and the SR to enable proximity of LTCCs in the plasma membrane with RyR2 channels in the SR (Valtonen et al. 2023). The formation and maintenance of these JMCs depend on junctophilin-2 (JPH2), which anchors the plasma membrane to the SR by binding to LTCCs and RyR2, together with caveolin-3 (Cav3) and striated muscle enriched protein kinase (SPEG) (Figure 2) (Landstrom et al. 2011; Beavers et al., 2014; Valtonen et al. 2023). JPH2 protein is therefore essential for facilitating the structural and functional interaction between LTCCs and RyR2, enabling

crosstalk between cell surface and Ca^{2+} signaling to ensure efficient Ca^{2+} release from the SR, during CICR (Valtonen et al. 2023; Landstrom et al. 2011).

Mechanical contraction of CMs is initiated when CICR mediated increased intracellular Ca^{2+} binds to troponin C (Eisner et al. 2017). In CMs, most of the cytoplasm, referred to as the sarcoplasm, is occupied by contractile myofilaments organized into sarcomeres (Pawlina 2024). These sarcomeres consist of thin actin filaments and thick myosin filaments, which together form the cardiac contractile machinery. During diastole, the interaction between actin and myosin is inhibited by troponin-tropomyosin complex. When Ca^{2+} binds to troponin C, it further induces conformational change in tropomyosin revealing myosin-binding sites on actin. This exposure allows myosin heads to bind to actin and form cross-bridges, resulting in sliding of the myofilaments and shortening of the sarcomeres during systole. Myosin functions with ATPase activity and the hydrolysis of ATP provides the energy required for CM contraction (Pawlina 2024). Resulted shortening of the CMs enables development of pressure within the ventricles and pumping of blood (Eisner et al. 2017). Following the systole, intracellular Ca^{2+} is decreased back to resting concentration leading to termination of the contraction and CM relaxation (Pawlina 2024).

1.1.3 Cardiac remodeling

The heart has the ability to adapt to changing physiological demands through structural remodeling of the myocardium (Samak et al. 2016). This remodeling can occur in response to increased mechanical or hemodynamic stress, such as during exercise or pregnancy, where enhanced cardiac performance is required. Under these physiological conditions, an important adaptive response is cardiac hypertrophy, which is typically mild and reversible. From a cellular perspective, physiological CM hypertrophy involves enlargement of individual cells, increased protein synthesis, and enhanced sarcomere organization. In contrast, prolonged pathological stress can lead to pathological hypertrophy, which is often associated with impaired cardiac function and myocardial fibrosis (Samak et al. 2016).

As noted above, hypertrophic growth can result from chronic pathological conditions such as hypertension (Samak et al. 2016). However, pathogenic genetic variants can also induce pathological hypertrophic growth in the absence of chronic hemodynamic stress (Marian & Braunwald 2017). This pathological hypertrophy is associated with structural remodeling of the myocardium, including ventricular hypertrophy, as well as presence of fibrosis and myocardial dysfunction. These changes are early indicators of pathological cardiac remodeling and may

contribute to progression toward heart failure. Due to hypertrophic growth in heart, the myocardial oxygen consumption increases, which can further worsen cardiac dysfunction and increase the risk of arrythmias, myocardial infarction and even sudden cardiac death. Consequently, pathological ventricular hypertrophy is regarded as an important predictor of cardiovascular morbidity and mortality (Samak et al. 2016).

The pathogenesis of pathological cardiac hypertrophy is complex, involving multiple cellular and molecular signaling pathways (Samak et al. 2016). First, mechanical stress activates mechanosensitive proteins within the sarcomeres, such as calsarcins, initiating hypertrophic signaling in CMs. Then, hormonal stimuli further influence hypertrophy through cell surface receptors, engaging downstream pathways such as transforming growth factor-beta (TGF-β), G-protein-coupled receptor cascades, and mitogen-activated protein kinases (MAPKs). Additionally, an important feature of pathological hypertrophy is inflammation, which involves immune cell infiltration, increased cytokine levels such as interleukin-6 (IL-6) and IL-1β, activation of inflammatory pathways, and promotion of fibrosis (Samak et al. 2016).

One hallmark of pathological hypertrophy is the reactivation of a fetal gene program (Samak et al. 2016). Metabolic remodeling accompanies these changes, with CMs shifting from fatty acid oxidation toward carbohydrate-dependent energy production, requiring changes in metabolic gene expression. Finally, oxidative stress, caused by increased reactive oxygen species (ROS), is also strongly associated with the pathogenesis of cardiac hypertrophy. ROS activate hypertrophic signaling pathways, including kinases such as tyrosine kinases and MAPKs. Additionally, ROS can impair cardiac contractile function by modifying proteins involved in ECC. ROS can also promote fibrotic remodeling through interactions with the ECM (Samak et al. 2016).

Important downstream consequence of pathological hypertrophy is myocardial fibrosis, where excessive deposition of ECM impairs cardiac function (Schlittler et al. 2023). In the myocardium, the ECM mainly consists of fibrillar proteins, particularly collagen type I and III, which are essential for the heart by providing structural support. In normal conditions, cFBs contribute to cardiac structural integrity through the regulation of ECM protein and enzyme synthesis and degradation. Moreover, cFBs have also essential role in maintaining the cardiac structure and function upon injury by migrating to the injury location and differentiating to myofibroblasts (myoFBs) that produce scar tissue to replace the dead cells. During pathological cardiac hypertrophy, excessive accumulation of ECM proteins occurs in the interstitial space,

the region between CMs, leading to interstitial fibrosis. This fibrotic remodeling affects cardiac function on multiple levels. First, excess fibrotic tissue stiffens the myocardium and therefore reduces ventricular compliance, impairing diastolic function. Second, interstitial fibrosis can disrupt electrical signals within the myocardium, increasing the risk of cardiac arrythmias (Schlittler et al. 2023).

Pathological fibrotic remodeling is largely driven by the activation of cFBs and their transition into myoFBs (Schlittler et al. 2023). The myoFB differentiation can be an outcome for many different stimuli, including cytokines, growth factors, mechanical stress and neurohormonal pathways, with TGF-β signaling pathway being the most important one. In this context, immune cells, CMs, ECs and even cFBs may all secrete growth factors and cytokines, such as TGF-β. TGF-β is initially secreted in latent form and stored in the cardiac tissue. Upon stimulation, TGF-β is activated by proteolytic cleavage. The bioactive TGF-β then binds cFB surface receptors, triggering canonical and non-canonical intracellular pathways that drive FB activation and differentiation into myoFBs, ultimately regulating transcription of profibrotic genes. Hence, when stimuli occur, cFBs proliferate, can migrate and eventually differentiate into myoFBs. Finally, these myoFBs drive ECM remodeling by upregulating genes such as *ACTA2* (Actin Alpha 2), which encodes the contractile protein alpha-smooth muscle actin (α-SMA), and *POSTN*, which encodes periostin, together with multiple other ECM proteins and remodeling enzymes (Schlittler et al. 2023).

1.2 Hypertrophic cardiomyopathy

1.2.1 Definition and clinical characteristics

Cardiomyopathies represent a major cause of heart failure and are defined as diseases of the myocardium associated with structural and/or functional abnormalities (Mosqueira et al. 2019). Among these, hypertrophic cardiomyopathy (HCM) is a hereditary cardiac disease characterized by asymmetrical thickening of the left ventricular wall, most severe in the interventricular septum, without abnormal loading conditions, such as hypertension, or identifiable phenocopies (Marian & Braunwald 2017; Vanninen et al. 2018; Mosqueira et al. 2019). In some patients, this localized left ventricular wall thickening obstructs blood flow from the left ventricle to the aorta via left ventricular outflow tract (LVOT) obstruction, causing hypertrophic obstructive cardiomyopathy (HOCM) (Dungu et al. 2024).

HCM is estimated to occur in approximately one in 500 adults, although more recent estimates place the prevalence closer to one in 200 (Hathaway et al. 2021). Among affected individuals, LVOT obstruction at rest is present in roughly one-third of cases and is inducible in another third (Marian & Braunwald 2017). Although HCM usually develops early in life at the cellular level, clinical symptoms may not appear until later in life, and some individuals remain asymptomatic throughout life (Maron & Maron. 2013). The most common symptoms of HCM include chest pain, shortness of breath during exertion, and abnormal heart rhythms, arrythmias. Moreover, while most patients are mildly symptomatic, in many young adults, the first symptom of HCM may be unexpected collapse and possible death. This makes HCM a well-recognized cause of sudden cardiac death among athletes and the most frequent cardiac cause of sudden death in young individuals (Maron & Maron. 2013).

Diagnosis of HCM relies on a combination of clinical assessment, imaging, and genetic testing (Marian & Braunwald 2017). Diagnosis of HCM is based primarily on cardiac imaging using echocardiography and, if needed, cardiac MRI (Moilanen et al. 2025). In adults, a localized wall thickness ≥15 mm is diagnostic and, if familial HCM variant is known the threshold lowers to ≥13 mm. In children, diagnosis requires maximum wall thickness exceeding the body surface area-corrected population mean by >2 standard deviations (Moilanen et al. 2025). In addition, genetic testing confirms the pathogenic variant and facilitates cascade screening of family members (Marian & Braunwald 2017). Furthermore, identifying affected patients and carriers early is essential for risk assessment and implementing strategies to prevent sudden cardiac death.

HCM is considered phenotypically heterogenous disease with variable disease expressivity as well as age-dependent, often incomplete penetrance. Thus, severe hypertrophy may be asymptomatic, whereas mild hypertrophy may be associated with significant arrhythmias, heart failure, and even sudden cardiac death (Hathaway et al. 2021). Although there is currently no curative therapy for HCM, several pharmacological and interventional treatment options are available that can relieve symptoms, reduce arrhythmic risk, and improve prognosis (Dungu et al. 2024). Moreover, in advanced HCM, myocardial fibrosis increases, and patients may develop heart failure, reduced left ventricular systolic function, and more severe arrhythmias, often leading to evaluation for heart transplantation in eligible patients (Dungu et al. 2024).

In HCM, left ventricular wall thickening primarily results from CM hypertrophy, which increases myocardial stiffness (Maron & Maron 2013; Marian & Braunwald 2017; Dungu et al.

2024). Together with myocardial disarray, this leads to diastolic dysfunction, which impairs ventricular filling and forces the heart to work harder to maintain cardiac output. Additionally, myocardial fibrosis is also a hallmark of HCM, and development of interstitial fibrosis further impairs cardiac function (Schlittler et al. 2023). In the context of HCM, fibrotic changes are most often observed in the septum and/or the left ventricle (Eijgenraam et al. 2020).

1.2.2 Genetics

The genetic basis of HCM is highly heterogeneous and involves variants in multiple gene encoding proteins that regulate cardiac structure and function (Maron & Maron 2013). Over the past two decades, more than 1400 pathogenic variants in dozens of genes have been identified, many of which are unique to individual families, illustrating both allelic heterogeneity, where different variants in the same gene can cause disease, and locus heterogeneity, where variants in different genes can also cause HCM (Maron & Maron 2013). HCM is most commonly inherited in an autosomal dominant pattern, although sporadic cases arise from de-novo variants (Maron & Maron 2013; Akhtar & Elliott 2018). Most of the pathogenic variants identified in patients with HCM are found in genes encoding thick and thin contractile cardiac sarcomeric proteins. However, variants in non-sarcomeric genes, including those involved in calcium handling and cytoskeletal organization, have also been identified. Additionally, certain metabolic and neuromuscular disorders, including Fabry disease and glycogen storage disorders, as well as genetic syndromes, such as Noonan syndrome, can mimic HCM phenotype and are hence referred to as HCM phenocopies (Maron & Maron 2013; Akhtar & Elliott 2018).

Genetic testing is recommended for all patients with a clinical diagnosis of HCM to identify diagnostic variants, confirm diagnosis, and enable screening of relatives (Hathaway et al., 2021). For genetic testing, targeted gene panels comprising dozens to over one hundred cardiomyopathy associated genes, as well as whole-exome sequencing, are commonly used (Moilanen et al. 2025). These variants are classified according to American College of Medical Genetics and Genomics (ACMG) guidelines, with pathogenic or likely pathogenic variants considered diagnostic (Hathaway et al. 2021). The diagnostic yield of molecular genetic testing in HCM is reported to be 25–40%, reflecting challenges in distinguishing genetic disease from acquired or systemic conditions and undiscovered disease genes or complex mechanisms (Vanninen et al. 2018). This complexity is further highlighted by the phenotypic heterogeneity of HCM, which arises from its complex genetic basis (Mosqueira et al. 2019). Beyond the pathogenic variant, factors such as the individual genetic and epigenetic background, together

with environmental modifiers, are thought to modulate the clinical phenotype (Mosqueira et al. 2019). Therefore, genetic testing also plays an important role by effectively excluding phenocopies that may require targeted therapies (Vanninen et al. 2018).

Pathogenic variants in sarcomeric protein genes account for the majority of HCM cases, representing approximately 40–60% of all HCM cases (Akhtar & Elliott 2018). Among patients with identified pathogenic variants, those in β-myosin heavy chain 7 (*MYH7*) and myosin-binding protein C (*MYBPC3*) together account for approximately 70% of cases. Additionally, other sarcomeric genes, such as cardiac troponin T2 (*TNNT2*), cardiac troponin I3 (*TNNI3*), alpha tropomyosin 1 (*TPM1*) and multiple other genes contribute less frequently, each accounting for 5% or fewer of cases (Akhtar & Elliott 2018). Out of the identified HCM variants, most are missense variants, substituting a single amino acid for another and potentially affecting protein structure and function (Marian & Braunwald 2017). Additionally, few HCM variants particularly in *MYBPC3* are frameshift variants or stop-gain/loss variants, which often result in absent or truncated protein.

A subset of HCM patients carry homozygous or compound heterozygous variants (more than one pathogenic variant in HCM-related genes) in sarcomeric genes, particularly in *MYBPC3*, which are associated with earlier disease onset and often more severe hypertrophy or fatal cardiomyopathy (Marian & Braunwald 2017; Vanninen et al. 2018). In addition, compound heterozygosity involving both sarcomeric and non-sarcomeric genes has been identified in HCM patients (Vanninen et al. 2018). However, these digenic variants do not seem to substantially worsen the core HCM phenotype. These non-sarcomeric pathogenic variants, particularly in genes regulating calcium handling, are increasingly recognized in HCM (Akhtar & Elliott 2018).

While many HCM associated variants are unique to individual families, founder effect contributes substantially to the variant spectrum in certain populations (Vanninen et al. 2018). Founder variants are pathogenic variants that originate from a single common ancestor and become enriched in isolated populations, accounting for a significant proportion of monogenic disease cases (Jääskeläinen et al. 2019). Due to Finland's unique population history, the spectrum of rare pathogenic variants in Finland differs from that of other European populations, and founder variants are relatively common in several monogenic diseases. In Finland, a substantial proportion of HCM cases is explained by a limited number of recurrent variants. The FinHCM study identified four major sarcomeric variants, *MYBPC3* (Gln1061Ter), *TPM1*

(Asp175Asn), *MYH7* (Arg1053Gln), and *MYH7* (Val606Met), accounting for approximately 28% of cases. Among these, *MYBPC3* (Gln1061Ter), *TPM1* (Asp175Asn), and *MYH7* (Arg1053Gln) are considered founder variants and together account around 24% of HCM cases (Jääskeläinen et al. 2019). More recently, a Finnish founder variant in the non-sarcomeric *JPH2* (Thr161Lys), has been identified in multiple families (Vanninen et al. 2018).

As disruption of JMCs is frequently observed in failing hearts, both reduced expression and variants in *JPH2* have been associated with heart failure and HCM (Vanninen et al. 2018). Although the first *JPH2* variant proposed as a candidate for HCM by Matsushita and colleagues (2007) was later shown to be a common polymorphism, subsequent studies have identified multiple other *JPH2* variants associated with HCM (Matsushita et al. 2007; Vanninen et al. 2018). Notably, Vanninen and colleagues (2018) reported the heterozygous missense variant *JPH2* c.482C>A, (Thr161Lys) in Finnish families as a monogenic cause of HCM, representing the first *JPH2* variant with demonstrated disease causality. They also linked this variant to the presence of fibrosis in the heart. Moreover, the variant is classified as pathogenic according to ACMG guidelines, based on strong co-segregation with the HCM phenotype, absence in reference populations, evolutionary conservation, and being deleterious in majority of *in silico* predictions (Vanninen et al. 2018).

Clinically, the *JPH2* (Thr161Lys) variant is associated to relatively early disease onset, with diagnosis on average at 27 years, distinguishing it from typical HCM and from the more common Finnish founder variants in *MYBPC3* and *TPM1* (Vanninen et al. 2018). Valtonen and colleagues (2023) further investigated the *JPH2* (Thr161Lys) variant using cardiomyocytes derived from patient-specific human induced pluripotent stem cells (hiPSCs). These cardiomyocytes exhibited key features of HCM, including cellular hypertrophy and arrhythmogenic activity. However, this model does not recapitulate myocardial fibrosis, limiting its ability to fully capture disease pathology. Together, these findings provide a basis for further investigation of the *JPH2* (Thr161Lys) variant and its role in HCM pathogenesis (Valtonen et al. 2023).

1.2.3 Pathogenesis

The pathogenesis of HCM involves diverse mechanisms corresponding to the heterogeneity of identified causal genes and variants (Marian & Braunwald 2017). In this context, the primary initiating event is a pathogenic variant in sarcomeric or non-sarcomeric gene, which can alter protein structure, function, or expression. In heterozygous missense variants, both wild-type

and mutant alleles are typically transcribed and translated, but allelic imbalance may alter the relative abundance of the mutant protein. Furthermore, incomplete compensation by the wild-type allele, together with variation in mutant protein stability and incorporation into sarcomeres and myofilaments, can lead to heterogeneous functional effects among CMs and may partly explain the variable phenotypic expression of HCM. By contrast, heterozygous variants affecting stop codons or frameshift variants commonly lead to reduced mutant mRNA and protein levels. In CMs, the quality control mechanisms detect these abnormal transcripts and prevent the synthesis of the truncated proteins by transcript degradation and proteolysis (Marian & Braunwald 2017).

The precise pathogenesis linking *JPH2* (Thr161Lys) variant to the HCM phenotype remains incompletely understood. However, the variant localizes to the joining domain, which directly interacts with RyR2, affecting a highly conserved amino acid across mammals (Figure 2) (Valtonen et al. 2023). It is known that JPH2 is essential for ECC by enabling efficient communication between LTCC and RyR2 within JMCs to ensure coordinated calcium signaling (Landstrom et al. 2011). Accordingly, increasing evidence implicates disrupted LTCC-RyR2 communication as a central mechanism in HCM pathogenesis.

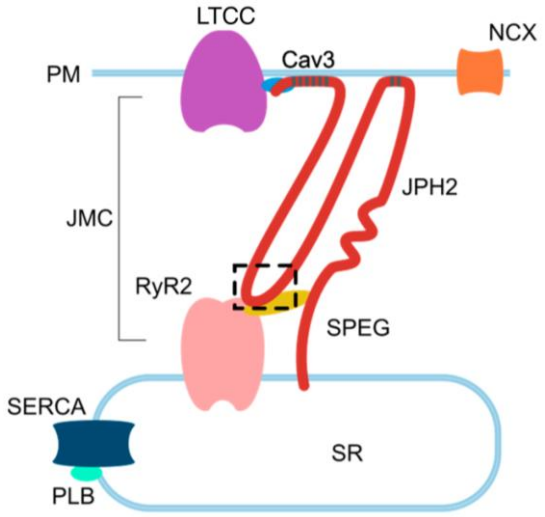

Figure 2. Schematic overview of junctophilin-2 (JPH2) localization within the junctional membrane complex (JMC) in a cardiomyocyte. The highlighted region shows the JPH2 joining region containing the *JPH2* (Thr161Lys) variant. PM, plasma membrane; SR, sarcoplasmic reticulum; LTCC, L-type Ca^{2+} channel; Cav3, Caveolin-3; NCX, sodium-calcium exchanger; JMC, junctional membrane complex; RyR2, ryanodine receptor 2; JPH2, junctophilin-2; SPEG, striated muscle enriched protein kinase; SERCA; sarcoplasmic reticulum Ca^{2+} ATPase; PLB, phospholamban. Adapted from (Valtonen et al. 2023) under CC BY 4.0 licence: https://creativecommons.org/licenses/by/4.0/.

Altered protein structure or reduced protein levels affect sarcomere function, calcium sensitivity, and ATPase activity (Marian & Braunwald 2017). These changes further activate compensatory responses by downstream signaling and alter transcriptional pathways, including calcium dependent, stress-responsive, epigenetic and noncoding RNA mediated mechanisms, which largely overlap with pathways activated in other forms of cardiac hypertrophy, such as pressure overload (e.g. TGF-β, calcineurin, and MAPK). The specific molecular responses depend on the function of the mutated gene. Eventually, activation of these pathways leads to changes in the myocardium, including CM hypertrophy and disarray, as well as interstitial fibrosis (Marian & Braunwald 2017).

The mechanisms linking HCM variants to myocardial fibrosis remain largely unclear (Schlittler et al. 2023). While fibrosis is often considered as a secondary response of CM hypertrophy, profibrotic signaling activates in HCM even prior to hypertrophic remodeling. TGF-β-driven fibroblast activation and myoFB differentiation are recognized as key drivers of fibrosis during HCM pathogenesis. In HCM, profibrotic signaling promotes ECM deposition, and fibroblast activation leads to the expression of proteins such as α-SMA, collagens, periostin, and integrins. However, the direct connection between HCM causing variants and fibroblast activation remains undefined, suggesting fibrosis may be an early disease hallmark (Schlittler et al. 2023).

Ultimately, these molecular and cellular changes in the myocardium manifest clinically as the hallmark features of HCM, including diastolic ventricular dysfunction, LVOT obstruction, imbalance between myocardial oxygen supply and demand due to initiation of fetal gene program resulting metabolic shift, arrythmias, and heart failure (Marian & Braunwald 2017).

1.3 Stem cells

Stem cells are undifferentiated cells with defining functional properties, including remarkable ability to self-renew, proliferate, and differentiate into specialized cell types (Poliwoda et al. 2022; Tian et al. 2023). In other words, stem cells are present throughout life in embryonic, fetal and adult tissues and are essential for both early development during neonatal stage and for tissue repair later in life in adult tissues (Poliwoda et al. 2022). Because of these unique properties, they are valuable for disease modeling, regenerative medicine, tissue repair, and drug discovery (Yin et al. 2016; Poliwoda et al. 2022; Tian et al. 2023). Stem cells are commonly classified based on their differentiation potential (potency) or their source of origin (Poliwoda et al. 2022).

Classification based on potency divides stem cells into totipotent, pluripotent, multipotent, oligopotent, and unipotent cells (Poliwoda et al. 2022). Totipotent stem cells have the highest differentiation capacity and can give rise to all cell types, including extraembryonic tissues. Pluripotent stem cells (PSCs) can differentiate into all the three embryonic germ layers (endoderm, mesoderm, and ectoderm) but cannot form extra-embryonic tissue. Multipotent stem cells can differentiate into multiple cell types within a specific tissue or lineage, whereas oligopotent stem cells can give rise to only a few related cell types and unipotent stem cells to a single cell type. Furthermore, with increasing differentiation, stem cells give rise to progenitor cells, which are more committed to specific cell types and have a more limited differentiation potential (Poliwoda et al. 2022).

Stem cells can also be classified according to their source (Yin et al. 2016). They can be obtained from various tissues and developmental stages, such as bone marrow, peripheral blood, adipose tissue, and amniotic fluid. These include adult stem cells, embryonic stem cells (ESCs), and iPSCs. Adult stem cells are found in adult tissues and are typically multipotent, oligopotent, or unipotent. They are an accessible and relatively ethically acceptable cell source with a lower risk of teratoma formation, and they can be isolated, modified, and transplanted back into the patient. ESCs are pluripotent cells derived from the inner cell mass of the blastocyst and can therefore give rise to nearly all cell types. However, their use raises significant ethical concerns related to ESC isolation from embryos. In contrast, iPSCs are generated from somatic cells and share many properties with ESCs but avoid the major ethical issues associated with ESCs (Yin et al. 2016).

In 2007, Shinya Yamanaka's group generated hiPSC for the first time from fully differentiated somatic cells, which transformed stem cell research and greatly advanced cardiac research beyond traditional animal and human tissue-based models. In this method, somatic cells are reprogrammed back into an embryonic-like state by overexpression of the transcription factors associated with pluripotency, *OCT3/4, SOX2, c-MYC*, and *KLF4*, under embryonic stem cell culture conditions (Takahashi et al. 2007). Since their first generation from mouse cells and later from human adult fibroblasts and other somatic cell types, iPSCs have become an important *in vitro* modeling tool to investigate also genetic diseases within their genetic background by using patient- and disease-specific iPSC lines (Takahashi & Yamanaka 2006; Takahashi et al. 2007; Yamanaka 2012; Cerneckis 2024).

Genome editing has further increased the value of iPSCs in research by allowing targeted gene correction, deletion, or insertion. This makes it possible to create reporter lines, knockout models, and isogenic control lines that differ only at the genetic variant of interest (Hockemeyer & Jaenisch 2016). Isogenic controls enable the study of genetic causality to understand also how other genes and epigenetics affect the pathogenic phenotype (Mosqueira et al. 2019). Earlier genome editing approaches included zinc finger nucleases and transcription activator-like effector nucleases, but these methods were time-consuming and less flexible (Hockemeyer & Jaenisch 2016). Nowadays, the CRISPR-Cas9 system has overcome many of these limitations and has become the most widely used genome editing platform in PSCs research.

Despite their many advantages, stem cell-based approaches also raise important concerns. When utilizing them for cell therapies, both ESCs and iPSCs are associated with an increased risk of tumorigenicity, as PSCs have the capacity for unlimited proliferation (Yamanaka 2020). Consequently, they may continue to proliferate after transplantation, potentially leading to teratoma or tumor formation. Additionally, immunogenicity remains an important concern because immune rejection is a critical issue in cell therapy. Although autologous iPSCs may reduce the risk, they do not fully eliminate immunogenic concerns (Yamanaka 2020).

In addition, iPSCs exhibit variability between cell lines due to factors such as donor origin, reprogramming method, clonal differences, and culture conditions. For example, epigenetic memory can influence their differentiation potential. This variability can lead to differences in morphology, growth, and gene expression, which may affect reproducibility and should be considered when interpreting results and in downstream applications (Yamanaka 2020).

1.4 Disease modeling of HCM

Despite advances in noninvasive cardiac imaging and monitoring, these approaches are limited in their ability to characterize the molecular mechanisms underlying HCM. Therefore, disease modeling for HCM is done with various *in vivo* and *in vitro* models to assess the HCM phenotype and identify new disease mechanisms and targets for improved HCM therapeutics (Table 1) (Mosqueira et al. 2019). Generated disease models aim to advance understanding of cellular and tissue-level alterations during HCM progression. However, experimental animal models incompletely recapitulate HCM progression due to species differences and lack of clinical complexity, while stem cell-derived models primarily capture variant-specific cellular changes and phenotypes (van den Dolder et al. 2025). Each of these models have distinct

strengths and limitations, suited to different research questions. Moreover, current disease models highlight key gaps for future disease models that are developed (Mosqueira et al. 2019).

Table 1. Disease models for studying HCM phenotypes. Created in BioRender.com.

Human tissue models	Animal models	Human iPSC-derived cardiac models	
		Cardiomyocytes (2D)	Heart organoids (3D)
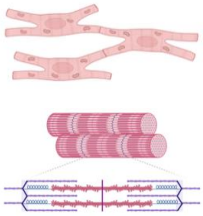			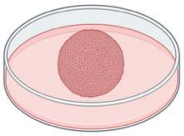

1.4.1 Human tissue and animal models

Earlier disease models based on intact heart muscle strips, isolated cardiomyocytes, skinned myofibrils and purified actin/myosin sarcomere proteins have played a major role in understanding the HCM progression and revealed disease hallmarks, making development of putative therapeutics possible (Mosqueira et al. 2019). These heart muscle derivates are directly isolated from patient's hearts. Intact heart muscle strips offer high physiological relevance, pharmacological predictivity and histology confirms key HCM hallmarks: fibrosis, CM hypertrophy and disarray. Isolated cardiomyocytes enable investigation of subcellular functions such as electrophysiology and Ca^{2+} handling in a level of single cells. Skinned myofibrils enable direct assessment of subcellular structures and myofilament function, revealing HCM specific contractile defects, including reduced Ca^{2+} sensitivity, ATP consumption, and overall ATP efficiency. Purified sarcomeric proteins provide direct assessment of actin-myosin interactions and give insights about contraction kinetics, ATPase activity and surrogate measure of force generation with better availability (Mosqueira et al. 2019).

In the context of models derived from human tissue, these approaches exhibit both distinct and shared limitations (Mosqueira et al. 2019). Most importantly, intact heart muscle strips, isolated cardiomyocytes and skinned myofibrils all have limited sample availability. Additionally, intact muscle strips require demanding logistics of tissue strips, while cardiomyocytes lack the proliferative ability in culture as well as 3D architecture and tend to dedifferentiate shortly after isolation. Skinned myofibrils and purified actin/myosin proteins are also prone to preparation

artefacts. Additionally, purified actin/myosin sarcomere proteins tend to generate less robust results due to absence of physiological complexity (Mosqueira et al. 2019).

Animal models are widely used in HCM research and have played a key role in advancing understanding of cardiac pathophysiology and in development of new therapies, as the fundamental mechanisms of cardiac excitation and contraction are relatively conserved across species (Mosqueira et al. 2019). Although mouse models are most commonly used, a wide range of species, including other rodents, domesticated animals, nonhuman primates, large animals, and nonmammals have been utilized in HCM studies (van den Dolder et al. 2025). Animal models enable whole organ or organism studies, are genetically modifiable, and provide ready access to cell and tissue samples (Mosqueira et al. 2019). Moreover, at the tissue level, they recapitulate key hallmark features of HCM, such as fibrosis and cardiomyocyte disarray, and allow investigation of functional parameters including contractility and calcium sensitivity (Mosqueira et al. 2019). In particular, transgenic mouse models have provided important insights into the cellular mechanisms of sarcomeric variants (van den Dolder et al. 2025). Therefore, despite a growing shift toward stem cell-derived models, which complement some limitations of animal models, *in vivo* systems remain essential for studying complex disease processes and for preclinical testing of novel therapeutics (van den Dolder et al. 2025).

As mentioned, there are also disadvantages when utilizing animal models to study HCM. Even though basic principles of cardiac excitation and contraction are relatively conserved among the species, still there is differences in cardiovascular physiology relative to human (Mosqueira et al. 2019). Particularly prominent differences are detected in mice, such as around 10 times faster heartbeat compared to human. Overall, species differences in gene expression relative to humans, together with inconsistencies across animal models, limit the translatability of these findings to the human disease phenotype. Furthermore, genetic manipulation is time-consuming when making animal models to study variant-specific HCM phenotypes (Mosqueira et al. 2019).

1.4.2 hiPSC-derived cardiomyocytes

In HCM research, hiPSCs have been particularly valuable because they can be differentiated into CMs that model the patient's genetic background and recapitulate many cardiomyocyte-specific features (Li et al. 2022). Although many HCM-causing variants have been identified, the pathogenic mechanisms linking genotype to phenotype remain incompletely understood. This is partly because previous animal models recapitulate human phenotypes only partially,

and human tissue samples are poorly available from different stages of HCM development. Myocardial tissue is usually obtained from patients with severe disease, so it often reflects advanced HCM rather than early disease stages, making it difficult to distinguish primary defects from secondary compensatory changes. Thus, hiPSC-based models have enabled efficient disease modeling of HCM and may help reveal disease mechanisms and patient-specific drug responses that were previously difficult to study (Li et al. 2022).

There are multiple differentiation methods available that result in hiPSC-derived CMs (hiPSC-CMs) (Mosqueira et al. 2019). These methods mimic heart development and guide hiPSCs through sequential differentiation stages, including mesoderm, cardiac mesoderm, and cardiac progenitor cells. The differentiation stages are induced by different growth factor mixtures in specific timepoints to form CMs (Mosqueira et al. 2019). Furthermore, these differentiation methods can be implemented using several approaches, including inductive coculture, embryoid body (EB) formation, monolayer culture, and suspension culture.

These differentiation methods provide a relatively pure and unlimited source of CMs that may recapitulate the patient-specific HCM genotype and when combined with CRISPR-Cas9, it allows direct comparison with isogenic controls to assess specific variant pathogenicity and pathogenesis (Mosqueira et al. 2019). To investigate the HCM pathogenesis in hiPSC-CMs, multiple phenotypic assays have been developed to assess structure, gene expression profiles, contractility, metabolism, electrophysiology, and calcium handling. However, *in vitro* studies with hiPSC-CMs cultured in 2-dimendional (2D) are limited to cardiomyocyte-specific phenotypes (Mosqueira et al. 2019).

Valtonen and colleagues (2023) characterized the *JPH2* p. (Thr161Lys) variant using CMs derived from patient-specific hiPSCs. These iPSC-CMs carrying the *JPH2* variant exhibited key features of HCM at both the structural and functional levels, including cellular hypertrophy, sarcomeric disarray, prolonged action potential duration, and arrhythmogenic activity. However, disease mechanisms remain poorly understood, as this 2D hiPSC models lack the ability to capture multicellular interactions driving disease progression. Therefore, further studies with more advanced models are essential to better characterize the HCM phenotype and to investigate the interplay between cardiomyocyte hypertrophy and fibrosis in the context of this *JPH2* variant (Valtonen et al. 2023). Although 2D models facilitate detailed analysis at the molecular, myofibrillar, and cellular levels, integration into organoids or engineered heart tissues (EHTs) also enables the investigation of tissue level properties (Mosqueira et al. 2019).

iPSC-derived cardiomyocytes generated using standard protocols remain distinct from adult cardiomyocytes in terms of morphology, sarcomeric protein isoform expression, electrophysiology, ECC, calcium handling, mitochondrial function, and metabolic profile (Li et al. 2022). Therefore, in iPSC-based disease modeling, one major challenge is that iPSC-derived cardiomyocytes often remain functionally and structurally immature compared with adult human cardiomyocytes, which can restrict the extent to which they recapitulate late-onset or fully developed cardiac phenotypes, associated with HCM (Li et al. 2022). However, measures are taken to enhance the maturation of hiPSC-CMs using biochemical approaches, environmental manipulation and 3-dimensional (3D) growth approaches (Machiraju & Greenway 2019).

Furthermore, hiPSC-CMs face additional limitations (Mosqueira et al. 2019). Although many protocols for cardiomyocyte differentiation from hiPSCs are generated to result large numbers of hiPSC-CMs, generally they are limited by presence of mixed subtype populations, variation between differentiation batches, scalability constraints, and interlaboratory variability due to the sensitivity of 2D cultures to changes in culture conditions. In the context of 2D cell cultures, they lack the multicellular cardiac composition in addition to hemodynamic and neurohormonal influences failing to fully model physiological complexity of the heart (Mosqueira et al. 2019). Overall, HCM modeling with iPSC-CMs remains in early stages, and the simplified *in vitro* environment may limit the ability of iPSC-CMs to fully recapitulate the HCM phenotype (Li et al. 2022). Nevertheless, iPSC-CM models are useful for studying HCM phenotypes and molecular mechanisms.

1.4.3 Heart organoids

Heart organoids are multicellular 3D *in vitro* tissue models derived from hiPSCs that capture essential features of structure and function of *in vivo* heart, enabling disease modeling (Fernandes et al. 2023). Heart organoids are used to model multiple different cardiovascular diseases including HCM (Buono et al. 2020; Ho et al. 2022; Lee et al. 2022). Heart organoids have gained great interest, as multicellular 3D cultures may improve the accuracy of disease modeling and drug testing by more closely resembling *in vivo* heart function by providing physiologically relevant microenvironment (Machiraju & Graanway 2019). Additionally, 3D culture systems are associated with enhanced maturation of hiPSC-CMs toward adult-like phenotype by creating an environment that more closely resembles *in vivo* heart development, further improving disease models. Moreover, organoid culture may enhance cell-cell

interactions within a multicellular cardiac environment and thereby increase the expression of genes associated with cardiomyocyte maturation, although the exact mechanisms remain unclear (Machiraju & Graanway 2019).

Heart organoid models range from spheroids consisting of only CMs to multicellular organoids that include CMs and supporting cardiac cell types, such as FBs and ECs, thereby better recapitulating the cellular complexity of the heart to mimic essential features of heart function (Lewis-Israeli et al. 2021; Fernandes et al. 2023; Idais et al. 2025). Multiple different heart organoid protocols have been established for disease modeling that could be used in HCM modeling. For example, Fernandes and colleagues (2023) developed a simplified organoid culture platform where hiPSC derived ventricular CMs and epicardial cells are combined. Within these organoids, epicardial cells further differentiate into cFBs and SMCs. The study also demonstrated that epicardial cells and their derivatives positively influence cardiomyocyte maturation (Fernandes et al. 2023). Lewis-Israeli and colleagues (2021) on the other hand developed self-assembling heart organoids platform, where organoids are generated from hiPSC EBs by utilizing Wnt signaling modulation. This protocol results multiple heart relevant cell types, including CMs, cFBs and SMCs (Lewis-Israeli et al. 2021).

Although *JPH2*-related HCM has been demonstrated in 2D hiPSC-derived CMs, corresponding heart organoid models have not yet been well established. However, disease modeling has been done to other HCM causing variants using heart organoids. For example, Desai and colleagues (2024) characterized the *MYBPC3* (D389V) variant HCM phenotype using heart organoids. These organoids contained CMs as well as supporting cell types, including cFBs and ECs. Compared with 2D CMs, the heart organoids showed upregulation of several genes associated with cardiac function. Importantly, organoids carrying the *MYBPC3* variant exhibited HCM phenotype at both structural and functional levels, including a hypercontractile phenotype and cellular hypertrophy. Moreover, the hypercontractile phenotype was rescued with the myosin inhibitor Mavacamten, highlighting the potential of organoids for drug testing in the future (Desai et al. 2024).

Despite many advantages, heart organoids also present challenges, including maintaining cardiomyocyte purity and viability, controlling aggregate size, and ensuring sufficient oxygen and nutrient diffusion (Machiraju & Greenway 2019). As organoids grow in size, limited oxygen and nutrient diffusion to the core may result in cell death. Additionally, in disease modeling, many experimental approaches might require single cell analyses to characterize

disease phenotypes. However, efficient dissociation and replating of 3D heart organoids are challenging, as a substantial proportion of cells do not survive the process. Moreover, variability in organoid size and cell number may lead to inconsistent phenotype manifestations as well as drug exposure, affecting the reliability of disease modeling and pharmacological studies (Machiraju & Greenway 2019).

1.5 Aims of the thesis

iPSC-based methods enable the study of genetic diseases in a patient-specific genetic background. HCM disease modeling is particularly important because the pathogenic mechanisms underlying the disease are still incompletely understood, and more advanced human-based models are needed to capture its complex, multicellular pathology. As introduced earlier, the *JPH2* (Thr161Lys) variant has previously been studied using patient-derived CMs. In the study by Valtonen and colleagues (2023), the results were promising, as the CMs recapitulated features of the HCM phenotype *in vitro*. However, disease modeling based on 2D cell culture has important limitations, particularly in HCM, where disease progression in cellular level includes not only cardiac hypertrophy, but also cardiac fibrosis. Therefore, interactions between multiple cardiac cell types, especially CMs and cFBs would be essential to study. Because the previous study did not capture multicellular interactions or fibrosis related features, it may not fully reflect the complexity of HCM pathogenesis. However, these findings provide a good basis for further investigation of the *JPH2* (Thr161Lys) variant and studies using more advanced models are needed to better characterize the phenotype associated with the *JPH2* (Thr161Lys) variant and to investigate the interplay between CM hypertrophy and fibrosis. Human heart organoids provide an opportunity to study these processes in a multicellular 3D system.

This thesis aims to characterize the phenotype associated with the *JPH2* c.482C>A (Thr161Lys) variant using patient-specific iPSC-derived human heart organoids. The specific aims are:

1. To generate human heart organoids from patient-specific iPSCs carrying the *JPH2* (Thr161Lys) variant.
2. To evaluate whether these organoids recapitulate structural and functional features of HCM, including hypertrophy and fibrosis related changes.

2 Materials and methods

2.1 Clinical information

To characterize the phenotype associated with the pathogenic *JPH2* (Thr161Lys) variant causing HCM, a hiPSC line derived from a male patient carrying the heterozygous alteration was used to generate human heart organoids (hHOs). At the age of 14, the patient was diagnosed with HCM, based on thickening of the interventricular septum (16 mm). However, the disease phenotype progressed with age and at the age of 16, thickening of the septum had increased (28 mm) and also elevated left ventricular outflow track (LVOT) gradient was measured. The patient exhibited ventricular arrythmias, including non-sustained ventricular tachycardias. Over time, the patient received several treatments, including β-blocker therapy starting at age 14, implantation of an intracardiac defibrillator at age 23, and alcohol septal ablation at age 24. As a control, isogenic gene-corrected hiPSC line with a restored cardiomyocyte phenotype as well as hiPSC line derived from a healthy 55-year-old female donor were used. The thesis was carried out under the existing ethical approvals of the Tampere University Heart Group for hiPSC culture and differentiation, with written informed consent obtained from all participants.

2.2 hiPSCs and cell culture

The hiPSC lines from the HCM patient UTA.09703.HCMJp (hereafter referred to as HCMJp), the isogenic control UTA.09701.iWT (hereafter referred to as iWT), and the healthy donor UTA.04602.WT (hereafter referred to as WT) were previously derived from dermal fibroblasts and characterized (Valtonen et al. 2023; Ahola et al. 2014). Human dermal fibroblasts were reprogrammed into hiPSCs using the four transcription factors *OCT4*, *SOX2*, *KLF4* and *c-MYC*. Introducing these transcription factors into donor cells induced their expression and reprogrammed the cells back to a pluripotent state (Takahashi & Yamanaka 2006; Takahashi et al. 2007).

The iWT line was modified from the HCMJp line by targeting the *JPH2* gene locus using CRISPR-Cas9 genome editing (Byrne et al. 2014). Briefly, a sequence-specific guide RNA (gRNA) was used to direct Cas9-mediated cleavage and enabled homology-directed repair using a repair template derived from healthy hiPSC genomic DNA. The detailed protocol is described by Valtonen et al. (2023). HCMJp and iWT hiPSC lines were characterized by Valtonen and colleagues by mutation analysis, gene expression analyses, including validation for pluripotency and detection of mutant and wild-type alleles in hiPSC-CMs, immunocytochemistry, karyotype and pluripotency analyses as well as differentiation of

cardiomyocytes (Valtonen et al. 2023). WT iPSC line was characterized by Ahola and colleagues using gene expression analysis for pluripotency validation, immunocytochemistry, karyotype analysis and ability to form EBs (Ahola et al. 2014).

To generate hHOs, HCMJp, iWT, and WT hiPSCs, kindly provided by PhD Martta Häkli as either cultured cells or frozen stocks, were used. All the cell lines were cultured under feeder-free conditions in 4 ml/well of mTESR1 medium (Stemcell Technologies, 85850), consisting of basal medium and supplement, and supplemented with 50 U/ml Penicillin/Streptomycin (Euroclone, ECB3001D) (hereafter referred to as mTeSR1) in 6-well plates (Corning, 3506) in Thermo steri-cycle i160 CO_2 humified incubator (37 ˚C, 5% CO_2) enabling the hiPSCs to proliferate while maintaining their pluripotent state. All cell cultures were maintained under identical incubation conditions.

The frozen hiPSCs in 1 ml stock were thawed in 37 ˚C water bath until almost completely thawed and transferred into 10 ml of mTeSR1. The cell suspension was centrifuged (200 × g, RT, 5 min) to remove the dimethyl sulfoxide (DMSO, Sigma-Aldrich, D2650) containing freezing medium and then resuspended in fresh mTeSR1 medium. The hiPSCs were seeded in 2 ml/well of mTeSR1 containing 2.5 µl/ml of iMatrix-511 (Amsbio, AMS.892-012) to support hiPSC adhesion into 6-well plates. When the hiPSC monolayers reached confluence, hHO generation was initiated or the cells were passaged. The hiPSCs were passaged by incubating the cells with Versene (Gibco, 15404033) (37 °C, 5-8 min) until the monolayer began to detach. Versene was aspirated, and cells were resuspended in mTeSR1 supplemented with 2.5 µl/ml iMatrix-511. Cells were fully detached using a cell scraper (Starstedt, 83.3950) and transferred to fresh mTeSR1 with iMatrix-511 before seeding at 2 ml/well in 6-well plates. A day after seeding, another 2 ml/well of mTeSR1 was added. During hiPSC culture, the medium was changed three times per week by removing 2 ml/well of old medium and adding 2ml/well of fresh mTeSR1.

2.3 Generation of human Heart Organoids (hHOs)

For the generation of hHOs, published protocol was used with small modifications (Figure 3) (Lewis-Israeli et al. 2021). Generation of hHOs was started when iPSC culture confluency reached 60-80%. iPSCs were incubated with Versene (37 ˚C, 5-8 min) until the monolayer started to detach. Versene was aspirated, and cells were resuspended in mTeSR1 using a cell scraper. Dissociated cells were counted using 0.4% Trypan Blue (Invitrogen, T10282) with a Countess 3 Automated Cell Counter (Thermo Fisher Scientific). For HCMJp hiPSCs, 2250 live

cells/well and for both, iWT and WT hiPSCs, 3375 live cells/well were seeded in 100 µl/well of mTeSR1 containing 5 µM ROCK inhibitor (Y-27632 Dihydrochloride, Selleck Chemicals, S1049) into pHEMA (50 g/l, Poly(2-hydroxyethyl methacrylate), Sigma-Aldrich, P3932-10G, dissolved in 95% ethanol) coated round bottom 96-well plate (Corning, 3799). The pHEMA coating was used to prevent hiPSC attachment to the bottom of the plate. The hiPSCs were centrifuged (100 × g, RT, 3 min) and incubated 48 h to allow EB formation in each well. After the first 24 h, 50 ml/well of medium was removed and 200 ml/well of fresh mTeSR1 was added to obtain a final volume of 250 µl/well.

The number of hiPSCs used for hHO generation was initially optimized in previous work by PhD Martta Häkli and subsequently refined in this thesis, using lower cell numbers than described in the original protocol (Lewis-Israeli et al. 2021). Initially, 3000 cells per well were seeded without accounting for cell viability. To reduce variation in viability during seeding, viable cells were subsequently quantified, and 2250 live cells/well were used to ensure consistent organoid size based on an average cell viability of 75%. Additionally, seeding numbers were further optimized for each hiPSC line to account for line-specific differences in viability during hHO generation. Both iWT and WT lines exhibited lower survival rates due to increased cell loss during early steps of the hHO formation and therefore, 3375 live cells/well were used to achieve comparable hHO formation efficiency and size.

Shortly, the hHO generation relied on three sequential Wnt signaling modulation steps at predefined time points on suspension EBs. Each time the medium was changed, 166 µl/well (around 2/3 of the total well volume) was removed and replaced with fresh medium. During the first step (day = D0), Wnt activation, EBs were incubated 24 h in humified incubator in 3-5 µM CHIR99021 (Tocris, 4423) (hereafter referred as CHIR), 1.25 ng/ml BMP4 (R&D Systems, 314-BP) and 1 ng/ml Activin A (Peproteck, 120-14E-50UG) in RPMI/B27 minus insulin medium consisting of basal medium RPMI 1640 + GlutaMAX (Gibco, 61870044), 2% B27 minus insulin Supplement (Gibco, A1895601), and supplemented with 50 U/ml Penicillin/Streptomycin (Euroclone, ECB3001D) (hereafter referred to as RPMI-ins) to induce mesoderm formation. After the incubation (D1), hHOs were kept 24 h in RPMI-ins. For the second step (D2), Wnt inhibition, EBs were incubated 48 h in 2 µM Wnt-C59 (R&D Systems, 5148) in RPMI-ins to induce cardiogenic mesoderm formation. After that (D4), hHOs were cultured in RPMI-ins for 48 h and then (D6) switched to RPMI/B27 with insulin for 24 h. The RPMI/B27 with insulin medium consisted of basal medium RPMI 1640 + GlutaMAX (Gibco, 61870044), 2% B27 Supplement (Gibco, 17504044), and supplemented with 50 U/ml

Penicillin/Streptomycin (Euroclone, ECB3001D) (hereafter referred to as RPMI). During last step (D7), Wnt activation, hHOs were incubated 1 h in 2 μM CHIR in RPMI for epicardial induction. After third activation, hHOs were cultured 48 h in RPMI. Thereafter (D9 onward), medium was changed three times per week around the same time. More detailed protocol can be found from (Lewis-Israeli et al. 2021).

During the first Wnt signaling activation step (D0), hHO generation for the HCMJp and WT lines was optimized by determining the optimal concentration of CHIR, a Wnt signaling activator. This factor is critical for successful organoid formation, as it induces mesoderm and cardiac mesoderm formation (Lewis-Israeli et al. 2021). In the first round, four concentrations were tested: 1 μM, 2 μM, 3 μM and 4 μM. As higher concentrations resulted more beating organoids, second round was performed using three CHIR concentrations: 4 μM, 5 μM and 6 μM to further improve hHO formation efficiency. In both rounds, beating activity of the hHOs was monitored until D15. hHOs were fixed on D15 and immunocytochemistry was utilized to assess the hHOs structurally. The optimal concentrations for both hiPSC lines were then utilized. For HCMJp, 4 μM and 5 μM CHIR were used whereas for WT, 3 μM and 4 μM CHIR were used. WT hiPSCs showed low hHO formation efficiency. Therefore, iWT line was subsequently used. Concentrations of 4 μM and 5 μM CHIR were used for this line, as it was derived from the HCMJp line and was therefore expected to behave similarly.

In addition, hHOs exhibited reduced beating activity after D15. To optimize the beating duration, for half of the hHOs, RPMI was maintained according to the original protocol (Lewis-Israeli et al., 2021), while the other half was changed and kept in 20% EB medium (composition for 50 ml of 20% EB medium: 38.75 ml basal medium KO-DMEM (Gibco, 10829018), 10 ml Fetal Bovine Serum (FBS, Gibco, A5669701), 0.5 ml MEM Non-Essential Amino Acids (NEAA, Gibco, 11140050), 0.5 ml GlutaMAX (Gibco, 35050038), and supplemented with 50 U/ml (0.25 ml) Penicillin/Streptomycin (Euroclone, ECB3001D) (hereafter referred to as 20% EB).

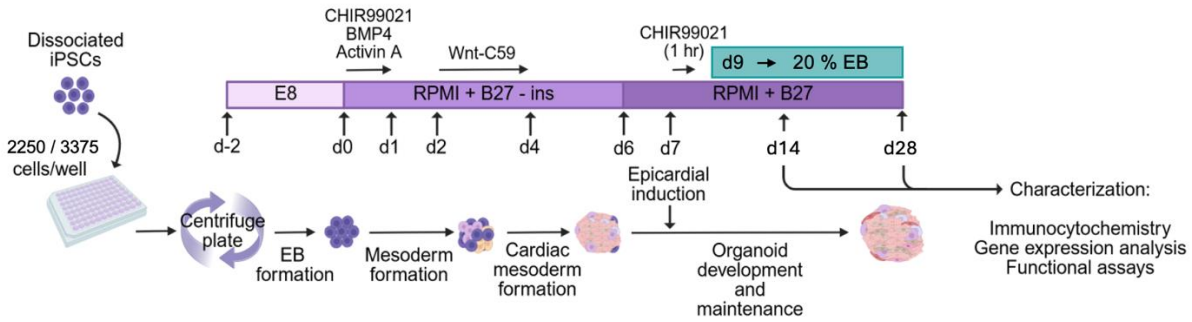

Figure 3. Schematic overview of human heart organoid generation protocol. Created in BioRender.com (adapted from Lewis-Israeli et al. 2021).

2.4 Characterization of organoids

To characterize the HCM phenotype of iPSC-derived hHOs structurally and functionally, the following analyses were utilized. Immunocytochemistry was performed to characterize the cardiomyocyte structure, cellular composition, and ECM of hHOs. Gene expression analysis was used to characterize the cellular composition, and hypertrophy and fibrosis markers of hHOs. Lastly, video-based analysis was used to assess the contractility of hHOs. Two timepoints, day 14 and day 28, were used for phenotypic characterization. Beating (B) or non-beating (NB) status of the hHOs was assigned based on visual inspection on day 14, although none of the organoids were beating on day 28.

On day 14, videos were taken from the hHOs before half of the hHOs were collected for immunocytochemistry and gene expression analyses. Video analysis was performed for HCMJp hHOs in all four conditions (4 µM CHIR 20% EB, 5 µM CHIR 20% EB, 4 µM CHIR RPMI, and 5 µM CHIR RPMI) but for iWT hHOs, it was done for 5 µM 20% EB condition as organoids only differentiated with 5 µM CHIR were successful and iWT organoids cultured in RPMI were displaying weak beating. For immunocytochemistry, samples consisting of 1-3 hHOs were collected for each antibody staining. In total, 5-8 hHOs per condition were collected for immunocytochemistry. For gene expression analysis, pooled organoid samples consisting of 6-8 hHOs per condition were collected. For HCMJp hHOs, only B organoids were collected from all conditions, whereas for iWT hHOs, also NB organoids were collected for both analyses. Additionally, HCMJp samples included organoids differentiated in both 4 µM and 5 µM CHIR, cultured in either 20 % EB or RPMI. In contrast, iWT samples included organoids differentiated only with 5 µM CHIR, cultured either in 20 % EB or RPMI.

On day 28, videos were not taken because the hHOs had stopped beating. The number of organoids collected for each downstream analysis was similar as on day 14. For HCMJp hHOs,

identical samples were collected as on day 14. For iWT hHOs, similar samples were collected from 5 µM CHIR 20 % EB organoids, whereas for 5 µM CHIR RPMI organoids, similar samples were collected besides no B samples for immunocytochemistry or gene expression analysis.

2.4.1 Immunocytochemistry

hHOs were collected to 1.5 ml Eppendorf tubes using a 1000 µl pipette tip to prevent disruption of the hHOs, washed twice in PBS (Gibco, 14200-067) and fixed in 4% paraformaldehyde (PFA, Electron Microscopy Sciences, 15713-S) solution at RT for 30-45 minutes. After fixation, hHOs were washed 3 times in PBS and incubated in Permeabilization/blocking solution containing 5% Normal Donkey Serum (NDS, Merck, S30) and 1% Triton X-100 (Sigma Aldric, T8787) in PBS overnight at 4 °C on a shaker. This step allowed antibodies to access intracellular proteins and blocked nonspecific binding sites. hHOs were washed twice in antibody solution containing 0.2% Triton X-100, 0.1% BSA (Sigma-Aldrich, A7906) and 0.05% Tween20 (PBS-Tween tablets, Medicago, 09-9410-100) in PBS and divided to PCR tubes (Nippon Genetics, FG-016FC) based on primary antibody mixtures. Three primary antibody mixtures were diluted in antibody solution: mixture 1 contained 1:400 Troponin T (Abcam, ab8295) and 1:400 CD90/THY1 (Abcam, ab133350); mixture 2 contained 1:400 MYBPC3 (Santa Cruz Biotechnology, sc-166081) and 1:400 TAGLN (Abcam, ab14106); and mixture 3 contained 1:400 Troponin T (Abcam, ab92546), 1:400 WT1 (Abcam, ab89901), and 1:200 MLC2A (Synaptic Systems, 56F5). For each antibody staining, 1-3 hHOs from all collected conditions were used. Primary antibody mixtures were added into the tubes and incubated for 24 h at 4 °C on a shaker.

Next day, the hHOs were washed three times for 5 min each in antibody solution and incubated with donkey-derived secondary antibodies corresponding to the species of the primary antibodies. Secondary antibody mixtures were diluted (1:400) in Secondary antibody solution containing 10% NDS, 0.2% Triton X-100, 0.1% BSA and 0.05% Tween20 in PBS. Secondary antibody mixtures 1 and 2 contained anti-mouse Alexa 488 (Invitrogen, A21202) and anti-rabbit Alexa 568 (Invitrogen, A10042), whereas mixture 3 contained anti-goat Alexa 488 (Invitrogen, A11057), anti-rabbit Alexa 568 (Invitrogen, A10042), and anti-mouse Alexa 647 (Invitrogen, A31571). Secondary antibody mixtures were added into the tubes and incubated overnight, light-protected at 4 °C on a shaker.

Lastly, hHOs were washed three times for 5 min each in antibody solution and nuclear counterstaining was done by incubating with Hoechst 33342 (ThermoFisher Scientific, H1399) (1:1000 in PBS) light-protected for 15-20 min at room temperature on a shaker. Finally, hHOs were washed twice for 5 min each with PBS and once for 5 min with Anti-adherence rinsing solution (Stemcell Technologies, 07010). hHOs were transferred to microscope glass, mounted with Vectashield Antifade Mounting Medium (Vector Laboratories, H-1000) and covered with coverslips. Additionally, small coverslips were used between the slide and coverslip to avoid disruption of the hHOs. Fluorescent images of the hHOs were taken with Evident FV4000 Laser Scanning Confocal Microscope (cellSens FV 3.1.1.67) using 10X magnification. Finally, images were modified using Fiji-ImageJ-64bit (Java 1.8.0_172).

2.4.2 Gene expression analysis

For gene expression analysis, total RNA was collected from the pooled hHO samples to yield enough RNA, and a total of 25 RNA samples were analyzed. The HCMJp hHOs included two B samples from each condition (20% EB 4 µM CHIR, 20% EB 5 µM CHIR, RPMI 4 µM CHIR, RPMI 5 µM CHIR) at both day 14 and day 28. The iWT hHOs included two B samples from 20% EB 5 µM CHIR, a NB 20% EB 5 µM CHIR sample, a B RPMI 5 µM CHIR sample, and a NB RPMI 5 µM CHIR sample at day 14 and similar samples from day 28 hHOs, without B RPMI 5 µM CHIR sample.

The RNA was extracted using RNeasy Mini Kit (Qiagen, 74104) with small modifications. Shortly, the hHOs were washed twice in PBS and then 700 µl/sample of QIAzol Cell Lysis reagent (Qiagen, 1023537) was added. Samples were vortexed 4-5 min to lyse the hHOs. Samples were stored in -80 °C until RNA extraction. If cell clumps remained, upon thawing of the samples, sonication (Bioruptor, UCD-200) was utilized to fully lyse the hHOs for optimal RNA yields. 140 µl of chloroform per sample was added, followed by incubation for 2-3 min and centrifugation (12000 × g, 4 °C, 15 min) to separate the aqueous RNA phase from the interphase and organic phase. The aqueous phase was collected and 1.5 volumes of Ethanol (ETAX, 64-17-5, 99.5%) was mixed with the samples. Up to 700 µl of the sample was transferred into RNeasy Mini Spin Columns placed in a 2 ml collection tube. Samples were centrifuged (8000 × g, RT, 30 s) and flow-through was discarded. This was repeated for the remainders of the samples. DNase digestion was done using RW1 buffer from the RNeasy Mini Kit to wash the samples but DNase I (5 µl/sample) and DNase I Reaction Buffer (75 µl/sample) from Total RNA Miniprep Kit (Monarch, T2010S) was utilized. DNase I incubation mix (80

µl/sample) was applied directly to RNeasy column membrane and incubated at room temperature for 15 min. Again, after the incubation, samples were washed with RW1 buffer from the RNeasy Mini Kit following washes with RPE buffer twice and once centrifuged empty (full speed, RT, 1 min) to dry the membrane. Finally, RNA was eluted by adding 30 µl/sample of RNase-free water directly to the spin column membrane and centrifuged (800 × g, RT, 1 min). Previous step was repeated using the eluate to achieve high concentration of RNA. RNA concentrations were measured with NanoDrop One (ThermoFisher Scientific). RNA samples were stored in -80 °C until reverse transcription.

Reverse transcription was performed to obtain complementary DNA (cDNA) from RNA samples using High-Capacity cDNA Reverse Transcription Kit (ThermoFisher Scientific, 4368814) with small modifications. Each reaction contained 500 ng of RNA and included 25 samples, Human Heart total RNA (Ambion, 7966), -RT, and water control. The reverse transcription master mix, consisting of RT Buffer, dNTP Mix (100 mM), RT Random Primers and MultiScribe Reverse Transcriptase, was prepared without RNase Inhibitor or water due to low RNA concentrations in some samples. Nuclease-free water was first added to MicroAmp 8-Tube Strip tubes (0.2 ml, Applied Biosystems, N8010580) according to the RNA concentration of each sample, followed by the addition of RNA samples. Lastly, 5.8 µl/tube of the master mix was added to the reactions to obtain reaction volume of 20 µl and reverse transcription was performed in a 2702 Thermal Cycler (Applied Biosystems) using the program shown in Table 2. The resulting cDNA samples were stored at -20 °C until qPCR.

Table 2. Thermal cycler program for reverse transcription.

Temperature	**Time**
25 °C	10 minutes
37 °C	120 minutes
85 °C	5 minutes
4 °C	Hold

Real-time quantitative PCR (RT-qPCR) was performed to analyze gene expression associated with cellular identity, hypertrophy, inflammation, and fibrosis in the hHOs using a 384-well plate (Bio-Rad, HSP3905) format. The cDNA obtained from the reverse transcription reaction was diluted 1:5 with nuclease-free water. In total, nine PCR reaction mixes were prepared, each

containing TaqMan Fast Advanced Master Mix (Applied Biosystems, 4444557), a specific TaqMan Gene Expression Assay (Applied Biosystems, Table 3), and nuclease-free water. Each reaction mix was prepared for three technical replicates of 25 samples, as well as Human Heart total RNA, -RT, and water controls. Subsequently, 9 µl of PCR reaction mix was added to each well, followed by the addition of 1 µl of diluted cDNA resulting in a final reaction volume of 10 µl. The reaction plate was sealed with optical adhesive film (Applied Biosystems, 4311971) and centrifuged briefly to bring the PCR reaction mix to the bottom of the well. RT-qPCR was performed in a CFX384 Real-Time PCR thermal cycler (Bio-Rad) using the program shown in Table 4.

Data acquired from RT-qPCR was analyzed by normalizing target gene expression to the housekeeping gene *GAPDH* (glyceraldehyde-3-phosphate dehydrogenase) and then to the control sample. *GAPDH* was used as it has been previously validated in the Heart group to exhibit stable expression in iPSC-CMs providing a reliable baseline for comparison (Häkli et al. 2021; Häkli et al. 2022). Its expression was comparable between samples also in the context of hHOs (data not shown). Relative gene expression levels were calculated using the ΔΔCt method as previously described (Winer et al. 1999) in Microsoft Excel (version 16.107.3). Technical replicates were averaged prior to analysis. Gene expression values (ΔCt) were first calculated by normalizing target gene expression to the housekeeping gene *GAPDH*. Then relative gene expression (ΔΔCt) was calculated as the difference between ΔCt values of each sample and the D14 iWT 5 µM EB B control sample. Relative gene expression of all samples from both time points (D14 and D28) were normalized to the same control sample to study the gene expression differences between conditions and time points. Relative expression levels (fold change) were calculated as $2^{-\Delta\Delta Ct}$. The fold change was compared between cell lines, experimental conditions, and time points. Due to limited number of biological replicates, no statistical analysis was performed for the data. The data was visualized using R (version 2026.01.2+418). Following R packages were used to visualize the data: readxl_1.4.5 (Wickham et al. 2026), dplyr_1.2.0 (Wickham et al. 2026), tidyr_1.3.2 (Wickham et al. 2025), stringr_1.6.0 (Wickham 2025), ggplot2_4.0.2 (Wickham et al. 2026), tidyverse_2.0.0 (Wickham 2023), and pheatmap_1.0.13 (Kolde 2025). Heatmap was drawn using the pheatmap function and columns and rows were clustered using standard parameters (clustering method = complete, clustering distance = Euclidean), and the data was scaled per gene (row).

Table 3. The amplified genes and the used TagMan Gene Expression Assays.

Function	**Gene**	**TaqMan Assay**
Housekeeping gene	*GAPDH*	Hs02758991_g1
Cellular identity	*TNNT2*	Hs00165960_m1
	WT1	Hs01103751_m1
	PECAM	Hs00169777_m1
	THY1	Hs00174816_m1
	ACTA2	Hs00426835_g1
Hypertrophy	*NPPB*	Hs00173590_m1
Inflammation	*IL6*	Hs00174131_m1
Fibrosis	*ACTA2*	Hs00426835_g1
	POSTN	Hs01566750_m1

Table 4. Thermal cycler program for RT-qPCR.

Real-time PCR system	**UNG incubation**	**Polymerase activation**	**PCR**	**40 cycles**
Temperature	Hold 50 °C	Hold 95 °C	Denature 95 °C	Anneal 60 °C
Time	2 min	20 sec	3 sec	30 sec

2.4.3 Video microscopy

Beating activity of hHOs was recorded using video microscopy with a Nikon Eclipse TS100-F microscope at 4X magnification. Twenty-second videos were captured at 100 frames per second from beating organoids. Three biological replicates were recorded for each condition. For the HCMJp line, all four conditions were recorded. For the iWT line, only the D14 5 µM CHIR 20% EB condition was recorded. Although iWT line differentiations were performed under identical conditions as HCMJp line, functionally successful differentiation was observed in only one condition (20% EB 5 µM CHIR).

Video-based contractility analysis was performed using MUSCLEMOTION ImageJ macro (version 1.0) (Sala et al. 2017; van Meer et al. 2018). Contraction duration, time to peak, relaxation time, and peak-to-peak time of beating hHOs were analyzed in Microsoft Excel. These parameters were compared across cell lines and experimental conditions, and statistical

analysis (Mann-Whitney test) was performed to determine whether there were statistically significant differences between all groups. Mann-Whitney test was utilized due to small sample size. Adjusted p-values were calculated using fdr method. Data was considered statistically significant at $p < 0.05$. Finally, the results were visualized using R. Following R packages were used to visualize the data: readxl_1.4.5, dplyr_1.2.0, stringr_1.6.0, ggplot2_4.0.2.

3 Results

3.1 Optimization of hHO generation resulted in reproducible and comparable heart organoid structure

The hHOs were generated from hiPSCs by self-assembly using a three-step Wnt signaling modulation. Optimization of hHO generation produced organoids with comparable structure and spontaneous beating. Modulation of the CHIR concentration during the D0 activation step enhanced cardiomyocyte content, and hHOs maintained spontaneous beating until D15. WT hiPSCs showed low hHO formation efficiency, so the D14 iWT 5 µM EB B hHOs were used as the control in all analyses. For the HCMJp line, 4 µM and 5 µM CHIR resulted in hHOs with robust beating and increased cardiomyocyte content compared to other tested concentrations. The same concentrations produced comparable outcomes in the control line. To account for line-specific differences in viability, the number of hiPSCs used for hHO generation were optimized for each cell line and resulted in comparable organoid formation and size (Figure 4). Phase contrast imaging over 14 days showed comparable efficiency and a notable increase in organoid size across cell lines and conditions, although organoids cultured in RPMI medium were slightly larger than those cultured in 20% EB medium (Figure 4). Optimization of culture media did not affect hHO beating duration, as organoids maintained in either RPMI or 20% EB medium stopped beating before day 28.

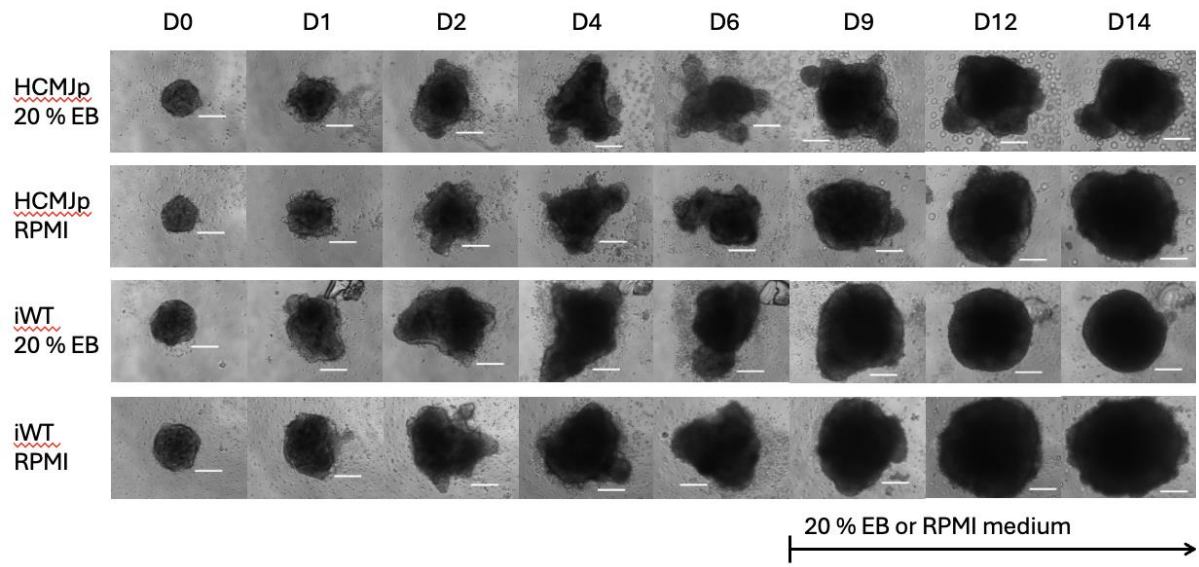

Figure 4. Reproducible generation of heart organoids with comparable size across conditions. Heart organoids were generated from HCMJp and iWT hiPSCs via self-assembly using three-step Wnt modulation (adapted from Lewis-Israeli et al. 2021). After generation, organoids were cultured in either 20% EB or RPMI medium from day 9 onward. Phase contrast images were taken over 14 days. Scale bar: 250 µm.

3.2 The hHO generation led to formation of multiple cardiac cell types

Cellular composition of the hHOs was assessed by confocal immunofluorescence imaging at day 14 and day 28 using markers for cardiomyocytes (Troponin T, MyBPC3), atrial cardiomyocytes (MLC2a), cardiac fibroblasts (CD90/THY1), smooth muscle cells (TAGLN), and epicardial cells (WT1). Confocal immunofluorescence imaging confirmed the presence of multiple cardiac cell types in hHOs (Figure 5). D14 and D28 heart organoids contained cardiomyocytes and cardiac fibroblasts, as well as smooth muscle cells (Figure 5A-B). Atrial cardiomyocytes were predominant at both time points, whereas epicardial cells were present only in low numbers (Figure 5C). Generally, no clear differences in cellular composition were observed between HCMJp organoids generated with 4 µM and 5 µM CHIR. However, more apparent difference was observed between organoids cultured in different mediums as cardiomyocytes were either localized in a single larger region or distributed across multiple smaller areas. The latter pattern was more frequently observed on day 14 organoids maintained in RPMI medium (Supplementary figure 1), whereas a single larger region was more typical of day 14 organoids cultured in 20% EB medium (Figure 5). Moreover, variability between individual organoids was evident.

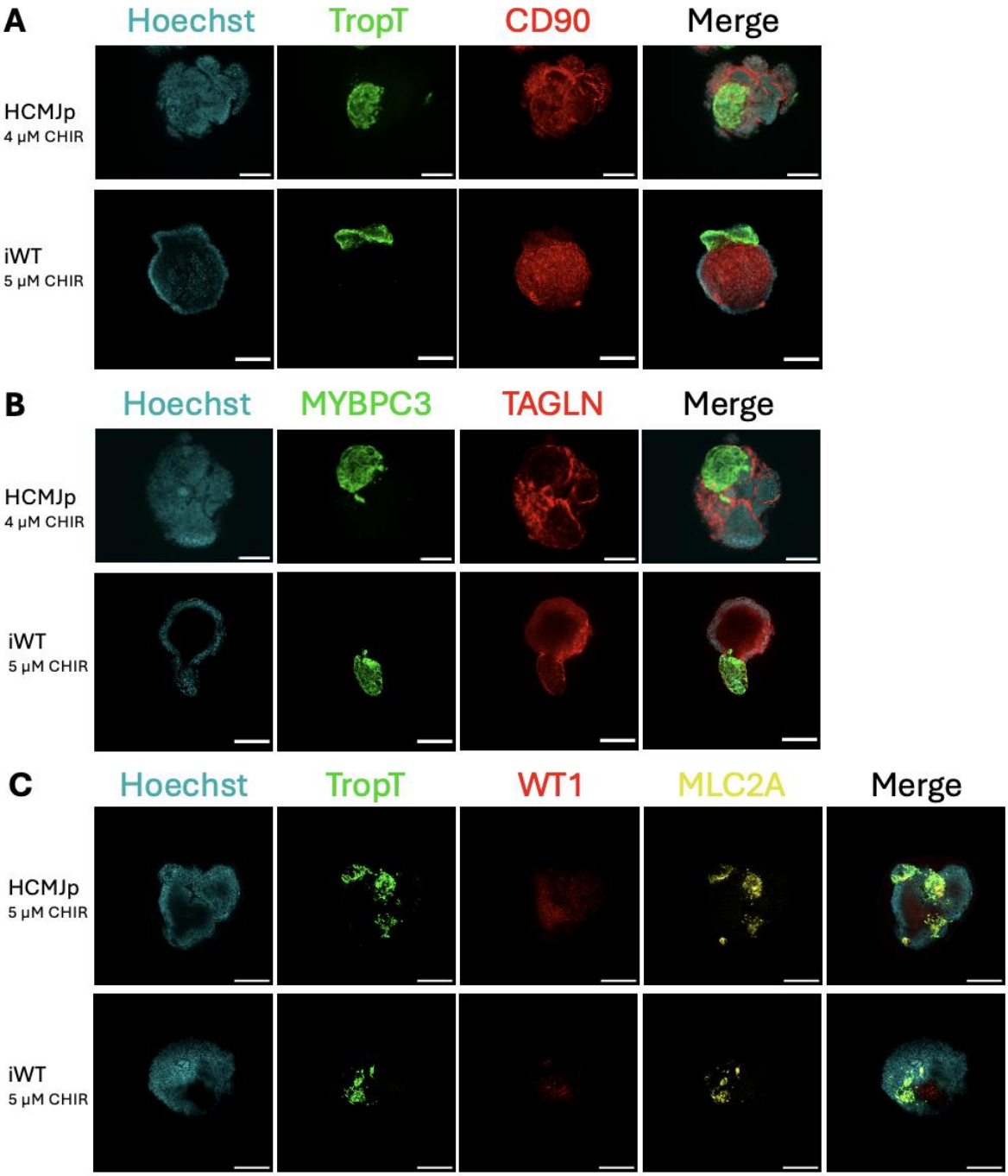

Figure 5. Heart organoids derived from HCMJp and iWT hiPSCs exhibit multiple cardiac cell types. Cellular composition was assessed using confocal immunofluorescence imaging at day 14 and day 28. All figures show heart organoids maintained in 20% EB medium. **A:** Day 14 heart organoids stained for Hoechst (blue, nuclei), TropT (green, cardiomyocytes), and CD90 (red, fibroblasts). **B:** Day 14 heart organoids stained for Hoechst (blue), MYBPC3 (green, cardiomyocytes), and TAGLN (red, smooth muscle cells). **C:** Day 28 heart organoids stained for Hoechst (blue), TropT (green), WT1 (red, epicardial cells), and MLC2A (yellow, atrial cardiomyocytes). Scale bar: 250 µm.

3.3 Gene expression patterns were predominantly associated with timepoint and culture medium rather than disease status

In HCM, the disease phenotype includes cardiomyocyte hypertrophy, cardiac fibrosis and increased inflammation. To investigate whether our model recapitulates the HCM phenotype at the transcriptional level, gene expression analysis was performed to assess the relative expression of genes associated with cellular identity, hypertrophy, inflammation, and fibrosis in hHOs at day 14 and day 28. Hierarchical clustering of the heatmap revealed no clear separation between HCMJp and control (iWT) organoid samples in gene expression patterns (Figure 6A). Instead, samples clustered primarily according to time point and culture medium. Several genes showed time point and culture medium dependent expression patterns. The cardiomyocyte marker *TNNT2* showed relatively higher expression in subset of D14 samples cultured in 20% EB, although variability between samples was observed. Notably, D14 5 µM RPMI HCMJp samples exhibited relatively the highest *TNNT2* expression. The hypertrophy marker *NPPB* (Natriuretic Peptide B) expression was also relatively elevated in a subset of D14 samples cultured in 20% EB. In contrast, the fibrosis marker *POSTN* exhibited relatively higher expression at D28 compared to D14 in all conditions. Similarly, the inflammation marker *IL6* (interleukin 6), epicardial marker *WT1* (Wilms tumor 1), and endothelial marker *PECAM1* (Platelet and Endothelial Cell Adhesion Molecule 1) showed relatively increased expression in D28 organoid samples cultured in 20% EB medium. The smooth muscle cell and fibrosis marker *ACTA2* expression was relatively higher in most of organoid samples cultured in 20 % EB. No clear expression pattern was observed for the cardiac fibroblast marker *THY1* (CD90).

Consistent with the clustering results, analysis of individual relative gene expression levels further revealed time point dependent changes across conditions (Figure 6B, Table 5). Because only the D14 sample was analyzed for iWT 5 µM RPMI B, time point dependent changes could not be examined. The cardiomyocyte marker *TNNT2* showed lower expression at D28 compared to D14. In contrast, the epicardial marker *WT1* exhibited increased expression at D28, particularly in HCMJp organoids cultured in 20% EB medium. Similarly, the fibrosis marker *POSTN* was upregulated at D28 in all samples, whereas *ACTA2* showed a slight decrease in HCMJp samples and a modest increase in iWT samples over time. The expression of inflammation marker *IL6* increased from D14 to D28 notably more in hHOs cultured in 20% EB medium compared to RPMI medium. Moreover, the highest levels were observed in 5 µM HCMJp organoids cultured in 20% EB medium.

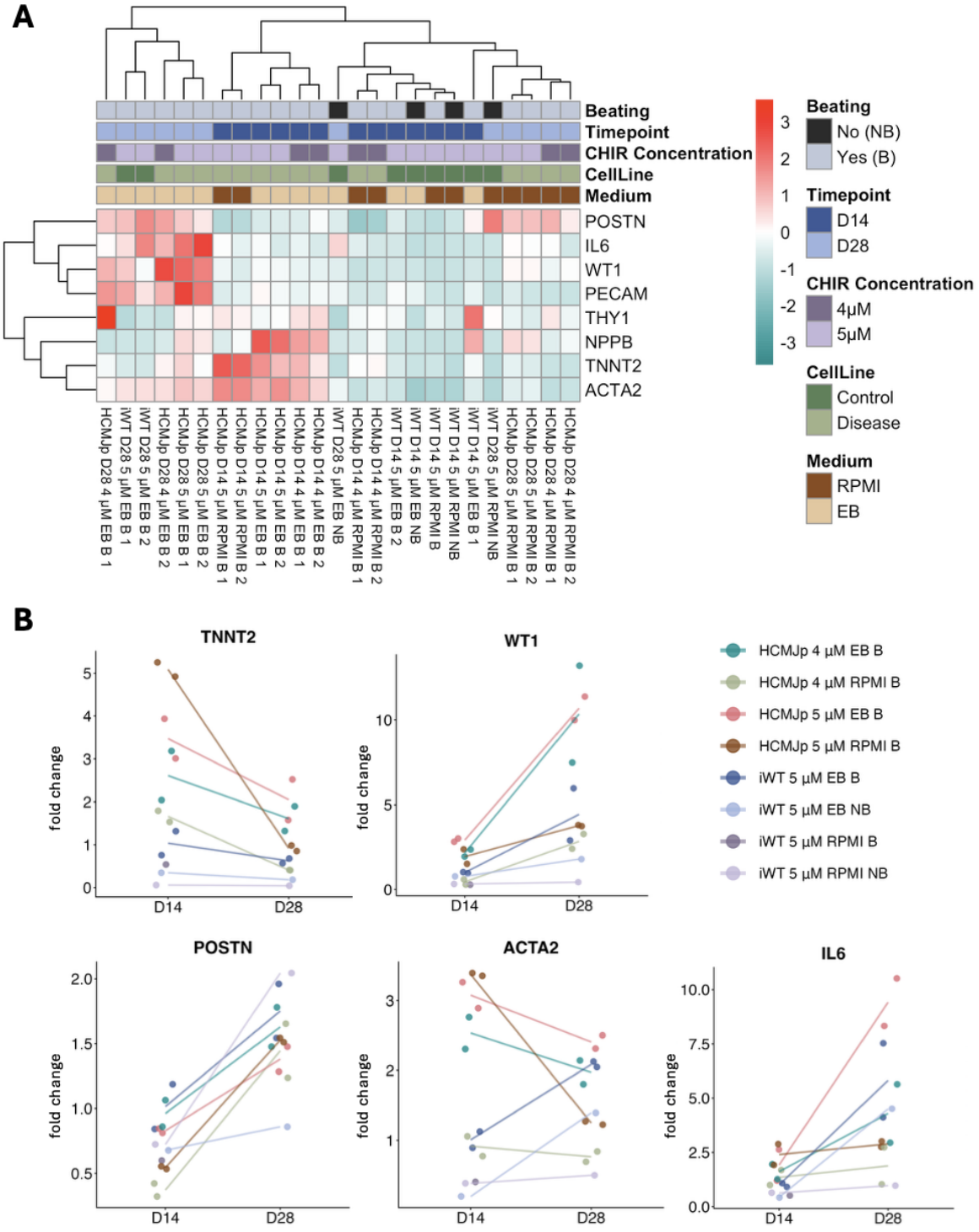

Figure 6. Gene expression patterns are associated with time point and culture medium rather than disease status. Relative gene expression of genes associated with cellular identity (*TNNT2, WT1, PECAM1, THY1, ACTA2*), hypertrophy (*NPPB*), inflammation (*IL6*), and fibrosis (*POSTN, ACTA2*) were analyzed at day 14 and day 28. Gene expression was normalized to *GAPDH*. Relative gene expression (fold change) for individual genes in heart organoid samples under different conditions was compared to the D14 iWT 5 µM EB B control sample. **A:** Heatmap showing gene expression across all heart organoid samples under different conditions. Expression values (fold change) were scaled per gene to highlight relative differences across samples. Hierarchical clustering was used to group similar

expression patterns. Color intensity represented relative gene expression levels. **B:** Fold changes were compared between timepoints. Changes revealed differences in cellular composition (*TNNT2, WT1, ACTA2*), inflammation (*IL6*) and fibrosis (*POSTN, ACTA2*) between HCMJp and iWT heart organoids over time. Lines connect mean values between timepoints for each condition, except for iWT 5 µM RPMI B of which only D14 sample was included.

Table 5. Fold change values of *TNNT2*, *WT1*, *POSTN*, *ACTA2*, and *IL6* in 8 samples at D14 and D28. Values are presented as mean ± std (n=2) or as single values (n=1).

Gene	Sample	D14		D28	
		mean	± std	mean	± std
TNNT2	HCMJp 4 µM EB B	2.61	0.81	1.61	0.41
	HCMJp 4 µM RPMI B	1.66	0.18	0.41	0.005
	HCMJp 5 µM EB B	3.47	0.65	2.05	0.67
	HCMJp 5 µM RPMI B	5.09	0.24	0.92	0.09
	iWT 5 µM EB B	1.04	0.40	0.62	0.08
	iWT 5 µM EB NB	0.35	-	0.18	-
	iWT 5 µM RPMI B	0.54	-	-	-
	iWT 5 µM RPMI NB	0.06	-	0.04	-
WT1	HCMJp 4 µM EB B	2.16	0.29	10.35	4.05
	HCMJp 4 µM RPMI B	0.45	0.22	2.85	0.61
	HCMJp 5 µM EB B	2.92	0.31	10.69	0.99
	HCMJp 5 µM RPMI B	1.95	0.61	3.78	0.04
	iWT 5 µM EB B	1.00	0.04	4.44	2.17
	iWT 5 µM EB NB	0.78	-	1.80	-
	iWT 5 µM RPMI B	0.28	-	-	-
	iWT 5 µM RPMI NB	0.33	-	0.44	-
POSTN	HCMJp 4 µM EB B	0.96	0.14	1.63	0.21
	HCMJp 4 µM RPMI B	0.37	0.07	1.44	0.29
	HCMJp 5 µM EB B	0.83	0.02	1.38	0.14
	HCMJp 5 µM RPMI B	0.54	0.01	1.53	0.02
	iWT 5 µM EB B	1.01	0.24	1.75	0.30
	iWT 5 µM EB NB	0.68	-	0.86	-
	iWT 5 µM RPMI B	0.60	-	-	-
	iWT 5 µM RPMI NB	0.72	-	2.04	-
ACTA2	HCMJp 4 µM EB B	2.53	0.32	1.97	0.24
	HCMJp 4 µM RPMI B	0.92	0.20	0.76	0.10
	HCMJp 5 µM EB B	3.08	0.26	2.41	0.13
	HCMJp 5 µM RPMI B	3.37	0.03	1.25	0.03
	iWT 5 µM EB B	1.01	0.16	2.08	0.06
	iWT 5 µM EB NB	0.20	-	1.39	-
	iWT 5 µM RPMI B	0.40	-	-	-
	iWT 5 µM RPMI NB	0.38	-	0.50	-
IL6	HCMJp 4 µM EB B	1.62	0.48	4.29	1.90
	HCMJp 4 µM RPMI B	1.35	0.48	1.88	1.19
	HCMJp 5 µM EB B	1.92	1.01	9.42	1.55
	HCMJp 5 µM RPMI B	2.41	0.68	2.89	0.18
	iWT 5 µM EB B	1.00	0.12	5.82	2.4
	iWT 5 µM EB NB	0.43	-	4.50	-
	iWT 5 µM RPMI B	0.52	-	-	-
	iWT 5 µM RPMI NB	0.63	-	0.97	-

3.4 Culture medium and potentially disease status affect heart organoid contractility

Functionally, the HCM phenotype is associated with diastolic dysfunction, characterized by impaired relaxation and prolonged relaxation kinetics. To assess whether the model exhibits a functional HCM phenotype, video-based contractility analysis was performed on spontaneously beating heart organoids. Peak to peak time, contraction duration, time to peak, and relaxation time were analyzed (Figure 7A). Although no statistically significant differences were observed in contractility parameters between the samples, there were observable trends in the data. As a control, D14 iWT 5 µM EB B hHOs were used. Peak to peak time varied between samples and was longest in control organoids (3536 ms ± 694) and shorter in HCMJp organoids (2388 ms ± 652 for 4 µM EB, 1557 ms ± 740 for 4 µM RPMI, 2654 ms ± 199 for 5 µM EB, and 1169 ms ± 73 for 5 µM RPMI) (Figure 7B). Contraction duration differed between conditions and was particularly altered in 5 µM HCMJp organoids compared to control (542 ms ± 188), being shortest in organoids maintained in RPMI medium (372 ms ± 12) and longest in those cultured in 20% EB medium (671 ms ± 70) (Figure 7C). Time to peak was also altered in HCMJp organoids compared to control (193 ms ± 78). In particular, 5 µM HCMJp organoids cultured in 20% EB medium showed slower and prolonged contractions (245 ms ± 54), whereas other HCMJp conditions exhibited faster contractions kinetics (150 ms ± 12 for 4 µM EB, 120 ms ± 30 for 4 µM RPMI, and 114 ms ± 6 for 5 µM RPMI) (Figure 7D). Relaxation time was similarly altered in 5 µM HCMJp organoids compared to control (349 ms ± 122). HCMJp organoids cultured in 20% EB medium showed also slower and more prolonged relaxation (426 ms ± 26), whereas organoids maintained in RPMI exhibited faster relaxation kinetics (258 ms ± 9) (Figure 7E).

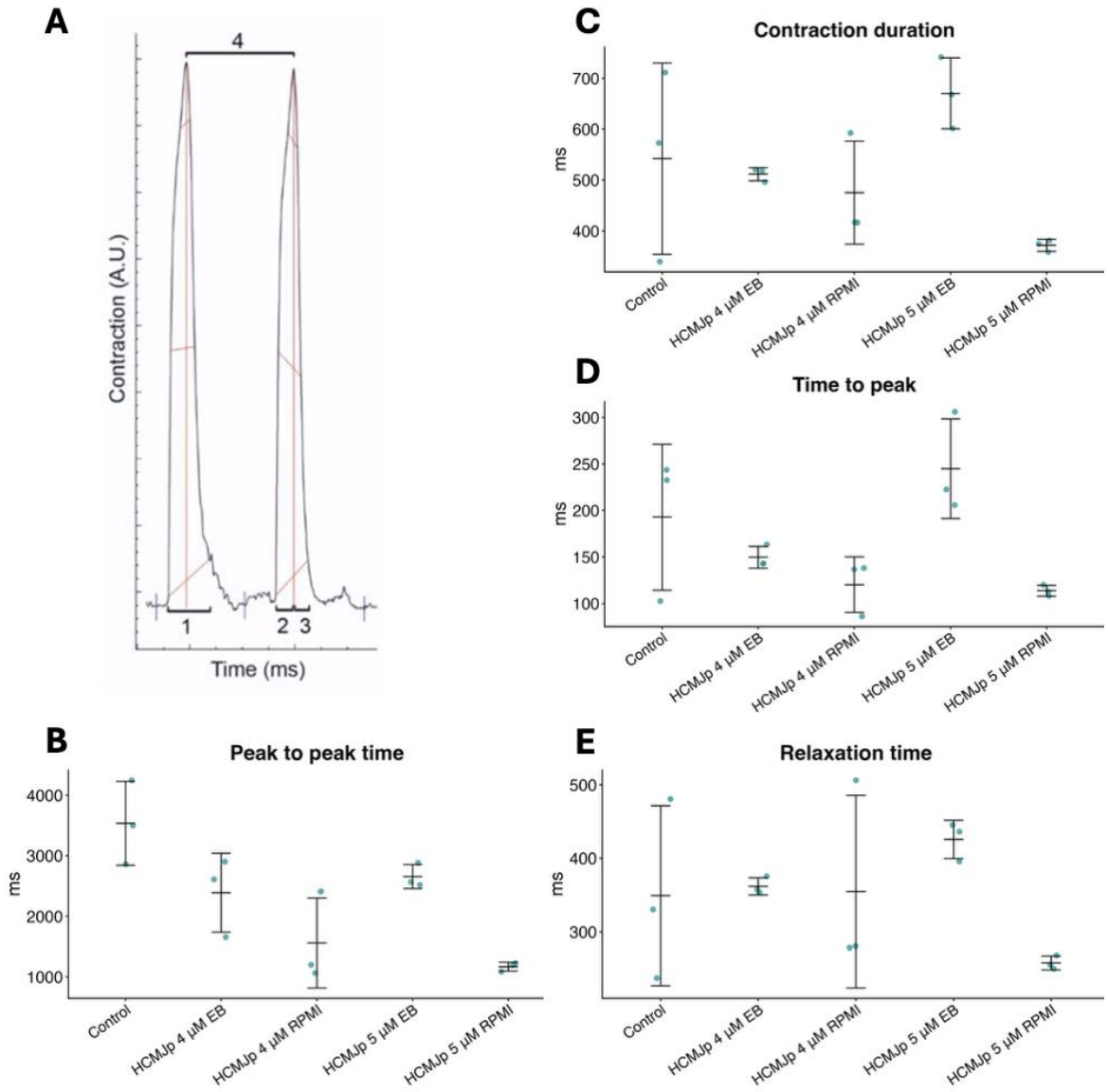

Figure 7. Disease and culture conditions affect contractile behavior in spontaneously beating heart organoids. Contractility was assessed using video microscopy recordings of spontaneously beating heart organoids under different conditions. **A:** MUSCLEMOTION was used to quantify contraction duration (1), time to peak (2), relaxation time (3), and peak to peak time from video recordings (adapted from Häkli et al. 2022 under CC BY 4.0 license: https://creativecommons.org/licenses/by/4.0/). **B:** Peak to peak time, **C:** contraction duration, **D:** time to peak, and **E:** relaxation time were analyzed across conditions (n = 3 heart organoids per condition). As a control, D14 iWT 5 µM EB B organoids were used. Statistical analysis (Mann-Whitney test) revealed no statistically significant differences between groups.

4 Discussion

This thesis aimed to generate patient-specific iPSC-derived hHO model to investigate and characterize the HCM phenotype of the *JPH2* (Thr2161Lys) variant. The hHOs were successfully generated from patient-specific iPSCs using a self-assembly platform and small molecule modulation of Wnt signaling (Lewis-Israeli et al. 2021). The resulting hHOs, regardless of used CHIR concentration, showed comparable structure and size, with multiple cardiac cell types, including CMs, cFBs, SMCs (Figure 4 & 5). Moreover, CMs exhibited spontaneous beating for over 15 days of culture.

However, at the transcriptional level, the gene expression patterns suggest that the hHO phenotype is influenced more by time point and culture medium than by disease status (Figure 6). CM marker *TNNT2* showed decreased expression over time and similar pattern was seen in hypertrophy marker *NPPB* expression. Therefore, the data suggests that cellular hypertrophy was not induced. Increased expression of fibrosis markers *POSTN* and *ACTA2* are associated with excessive accumulation of ECM (Schlittler et al. 2023). Hence, these genes were investigated to reveal whether fibrosis was induced in the hHOs. *POSTN* showed slightly increased expression over time in all samples, although change was likely too small to be biologically significant, whereas *ACTA2* expression did not follow this trend. Relative expression of *ACTA2* seemed to decrease over time in the HCMJp hHOs whereas slightly increase in control hHOs cultured in 20% EB medium (Figure 6B). However, *ACTA2* is also used as a marker gene for smooth muscle cells (Georgescu et al. 2015). Therefore, the changes in *ACTA2* expression might not be directly associated with fibrosis. Taken together, the data suggest that HCM induced fibrosis was not strongly induced in hHOs, although the presence of CMs and cFBs was confirmed (Figure 5A). The expression of *IL6* has been shown to directly promote hypertrophy (Samak et al. 2016). Expression of *IL6* showed clear increase over time in hHOs cultured in 20% EB medium, especially in 5 µM HCMJp hHOs. This indicates that 20% EB medium may affect hHOs by increasing inflammation related to HCM phenotype. Additionally, increased expression of *WT1* was seen over time particularly in 20% EB HCMJp hHOs at the transcriptional level (Figure 6B), although this was not seen in protein level (Figure 5C). Generally, staining of WT1 was relatively low in all immunocytochemistry samples (Figure 5C) (Supplementary figure 1).

Moreover, functional analysis of hHO contractile behavior revealed differences between culture conditions, suggesting that the culture medium and potentially disease status may affect the

contractile properties of spontaneously beating hHOs (Figure 7). Particularly 20% EB HCMJp hHOs showed slower and prolonged contractions, including delayed relaxation, suggesting that these hHOs may exhibit features of HCM phenotype associated with diastolic dysfunction. Taken together, despite the successful formation of hHOs, the HCM phenotype, including hypertrophy, fibrosis, and inflammation related changes, was not yet evident.

In a previous study by Valtonen et al. (2023), they characterized the *JPH2* (Thr2161Lys) variant using patient-specific 2D iPSC-CMs. These hiPSC-CMs exhibited an HCM phenotype, including structural features such as cellular hypertrophy and sarcomeric disarray (Valtonen et al. 2023). However, when using this same hiPSC line in hHO generation, gene expression analysis revealed no induction of cellular hypertrophy. This may be due to CM cell death or because CMs stop proliferating after differentiation, whereas other cell types in hHOs, such as epicardial cells, continue to proliferate, potentially hiding the hypertrophic effect. However, the study by Valtonen et al. (2023) did not investigate the interplay between hypertrophy and fibrosis in the context of this *JPH2* variant. Hence, this gap in knowledge gave motivation for this study to take place.

Several factors may explain why the HCM phenotype is not yet evident in hHOs carrying the *JPH2* (Thr2161Lys) variant. A challenge of hiPSC-derived cell models is that they remain structurally and functionally immature compared to adult cells *in vivo,* which may influence disease modeling accuracy. Although multiple studies suggest that 3D culture promotes the maturation of hiPSC-derived cardiac cells, including CMs, this remains an ongoing and incompletely understood area of research (Machiraju & Graanway 2019; Yang et al. 2023). Thus, resulting hHOs may contain cells that are too immature to fully recapitulate the complex HCM phenotype. Gene expression patterns are grouped according to time point (Figure 6), indicating that hHOs from the same timepoint are transcriptionally more like each other than those from different time point. This suggests ongoing developmental changes and potential maturation after the first timepoint (D14), although the hHOs appear structurally similar from D12 onwards (figure 4). Moreover, if maturation is required for manifestation of the HCM phenotype, longer culture time may be necessary to reveal phenotypic changes at the transcriptional level.

Also, the cellular composition of the hHOs could be improved to better recapitulate the HCM phenotype. The most abundant cell type in the heart is CMs with ventricular CMs comprising the majority present in the ventricles (Litviňuková et al. 2020). However, despite optimization

of the hHO protocol, the resulting hHOs contain fewer CMs compared to the *in vivo* heart (Figure 5). Moreover, atrial cardiomyocytes were predominant at both time points. As HCM primarily affects the ventricles (Marian & Braunwald 2017; Mosqueira et al. 2019; Dungu et al. 2024), a higher proportion of ventricular CMs in hHOs may improve the physiological relevance of the model. Additionally, by increasing the number of CMs, functional properties of hHOs may improve, including spontaneous beating duration. Functional properties could be also improved with culture conditions, including use of even more suitable culture medium. To conclude, by further optimizing the cellular composition by improving the CM content to the same level present *in vivo* ventricular myocardium and potentially further optimizing the culture conditions, these hHOs could more accurately recapitulate the HCM phenotype.

Although the HCM phenotype was not yet evident in the hHOs, this organoid model possesses potential. This self-organizing method, used to generate heart organoids, recapitulates human cardiogenesis (Lewis-Israeli et al. 2021; Yang et al. 2023). Moreover, it may have higher physiological relevance compared to 2D models, as multicellular 3D models more closely resemble *in vivo* morphology, a feature that has been linked to improved disease modeling and drug testing (Machiraju & Greenway 2019). Generally, heart organoids have been successfully used for HCM disease modeling. For example, Desai et al. (2024) demonstrated that heart organoids recapitulate the HCM phenotype and respond to drug treatment, highlighting their potential for disease modeling and drug testing (Desai et al. 2024). However, the diverse phenotypes and molecular mechanisms associated with different HCM variants complicate the identification of disease mechanisms and broadly effective treatment strategies (Ojala et al. 2016; Mosqueira et al. 2019). Therefore, it is important to investigate a wide range of HCM variants, including both common and rare forms, to ultimately understand the disease mechanisms and identify optimal treatments for most HCM patients.

As discussed above, even when using an already published protocol, the results reported in the original study may be difficult to replicate (Li et al., 2022). This challenge with hiPSC-derived cell models became evident when the previously published protocol could not be fully reproduced in this thesis, as cardiomyocyte content remained lower despite optimization compared to the hHOs reported by Lewis-Israeli and colleagues (2021). Furthermore, this highlights a broader issue of low reproducibility despite the availability of numerous protocols for generating iPSC-CMs and cardiac organoids. Moreover, this thesis showed that culture medium influences the hHO phenotype transcriptionally and functionally (Figure 6 & 7). Also, previous studies investigating iPSC-derived cardiomyocytes carrying HCM-associated variants

have reported substantial variability in phenotypic outcomes, including cell size and contractility, with no clear consensus across studies (Li et al. 2022). This variability likely reflects differences in culture conditions, differentiation protocols, and methods between laboratories. Taken together, these findings highlight the need for standardized and widely accepted approaches in iPSC-based disease modeling, as the lack of standard protocols may contribute to inconsistencies and limit reproducibility across studies (Li et al. 2022).

This study has limitations that may affect the interpretation of the results. The main limitation is the limited number of replicates, as optimization of the hHOs took longer than expected, which limited the opportunity to repeat the cultures and obtain a higher number of biological replicates. Therefore, the findings should be considered preliminary. Variability between organoids was observed and therefore, improved control over cell composition could enhance reproducibility and consistency of the results. Additionally, RT-qPCR of pooled organoid samples provides averaged gene expression across heterogeneous cell populations. Future studies could benefit from single cell approaches to better investigate cell type specific processes during HCM pathogenesis. In particular, scRNA-Seq (single-cell RNA sequencing) would enable the analysis of individual cell types within the organoids and potentially reveal interaction patterns between different cell populations, allowing more in-depth characterization (Tzec-Interián et al. 2025). Moreover, as an untargeted method, it could allow for new discoveries beyond predefined gene sets. In addition, the hHO model was studied in a simplified *in vitro* environment, lacking circulation and neurohormonal regulation. In the future, further optimization of this *in vitro* hHO model could include integration with organ-on-chip platforms to enhance its potential as a tool for disease modeling and drug testing. Integration with organ-on-chip platforms could enhance the physiological relevance of the model by enabling controlled fluid flow and mechanical stimulation (Liu et al. 2025).

5 Acknowledgements

First, I would like to thank my supervisors, Martta Häkli, Katriina Aalto-Setälä, and Heidi Viitaniemi, for their invaluable help and guidance throughout this master's thesis. I always received the support I needed.

I would like to give special thanks to Martta Häkli for involving me in her project and for teaching me many essential aspects of heart organoids. I also thank Katriina Aalto-Setälä and the entire Heart group at Tampere University for making this thesis possible and for introducing me to the fascinating world of hiPSCs. This journey has been an unforgettable experience!

I am deeply grateful to my family and friends for their continuous support throughout my studies and for always believing in me. Special thanks go to my sister for hosting me during my time in Tampere.

I also acknowledge the use of ChatGPT-5.5 (OpenAI) for language editing.

References

Ahola, A., Kiviaho, A.L., Larsson, K., Honkanen, M., Aalto-Setälä, K., Hyttinen, J., (2014). Video image-based analysis of single human induced pluripotent stem cell derived cardiomyocyte beat-ing dynamics using digital image correlation. BioMedical Engineering 13, 39. DOI: https://doi.org/10.1186/1475-925X-13-39

Akhtar, M., Elliott, P., (2018). The genetics of hypertrophic cardiomyopathy. Global Cardiology Science and Practice 3. DOI: https://doi.org/10.21542/gcsp.2018.36

Beavers, D.L., Landstrom, A.P., Chiang, D.Y., Wehrens, X.H.T., (2014). Emerging roles of junctophilin-2 in the heart and implications for cardiac diseases. Cardiovascular Research 103, 198–205. DOI: https://doi.org/10.1093/cvr/cvu151

Byrne, S.M., Mali, P., Church, G.M., (2014). Genome Editing in Human Stem Cellsm. Methods in Enzymology 504, 119–138. DOI: https://doi.org/10.1016/B978-0-12-801185-0.00006-4

Cerneckis, J., Cai, H., Shi, Y., (2024). Induced pluripotent stem cells (iPSCs): molecular mecha-nisms of induction and applications. Signal Transduction and Targeted Therapy 9, 112. DOI: https://doi.org/10.1038/s41392-024-01809-0

Desai, D., Song, T., Singh, R.R., Baby, A., McNamara, J., Green, L.C., Nabavizadeh, P., Ericksen, M., Bazrafshan, S., Natesan, S., Sadayappan, S., (2024). MYBPC3 D389V Variant Induces Hypercontractility in Cardiac Organoids. Cells 13, 1913. DOI: https://doi.org/10.3390/cells13221913

Dungu, J.N., Hardy-Wallace, A., Dimarco, A.D., Savage, H.O., (2024). Hypertrophic Cardiomyo-pathy. Current Heart Failure Reports 21, 428–438. DOI: https://doi.org/10.1007/s11897-024-00654-0

Eijgenraam, T.R., Silljé, H.H.W., De Boer, R.A., (2020). Current understanding of fibrosis in genetic cardiomyopathies. Trends in Cardiovascular Medicine 30, 353–361. DOI: https://doi.org/10.1016/j.tcm.2019.09.003

Eisner, D.A., Caldwell, J.L., Kistamás, K., Trafford, A.W., (2017). Calcium and Excitation-Contraction Coupling in the Heart. Circulation Research 121, 181–195. DOI: https://doi.org/10.1161/CIRCRESAHA.117.310230

Fernandes, I., Funakoshi, S., Hamidzada, H., Epelman, S., Keller, G., (2023). Modeling cardiac fibroblast heterogeneity from human pluripotent stem cell-derived epicardial cells. Nature Com-munications 14, 8183. DOI: https://doi.org/10.1038/s41467-023-43312-0

Filippo Buono, M., Von Boehmer, L., Strang, J., P. Hoerstrup, S., Y. Emmert, M., Nugraha, B., (2020). Human Cardiac Organoids for Modeling Genetic Cardiomyopathy. Cells 9, 1733. DOI: https://doi.org/10.3390/cells9071733

Georgescu, M.-M., Pinho, M.D.C., Richardson, T.E., Torrealba, J., Buja, L.M., Milewicz, D.M., Raisanen, J.M., Burns, D.K., (2015). The defining pathology of the new clinical and histopatho-logic entity ACTA2-related cerebrovascular disease. Acta Neuropathologica Communications 3, 81. DOI: https://doi.org/10.1186/s40478-015-0262-7

Gray, H., (2025). Gray's anatomy: the anatomical basis of clinical practice (Forty-third edition). Elsevier.

Harvey, P.A., Leinwand, L.A., (2011). Cellular mechanisms of cardiomyopathy. Journal of Cell Biology 194, 355–365. DOI: https://doi.org/10.1083/jcb.201101100

Hathaway, J., Heliö, K., Saarinen, I., Tallila, J., Seppälä, E.H., Tuupanen, S., Turpeinen, H., Kangas-Kontio, T., Schleit, J., Tommiska, J., Kytölä, V., Valori, M., Muona, M., Sistonen, J., Gentile, M., Salmenperä, P., Myllykangas, S., Paananen, J., Alastalo, T.-P., Heliö, T., Koskenvuo, J., (2021). Diagnostic yield of genetic testing in a heterogeneous cohort of 1376 HCM patients. BMC Cardiovascular Disorders 21, 126. DOI: https://doi.org/10.1186/s12872-021-01927-5

Ho, B.X., Pang, J.K.S., Chen, Y., Loh, Y.-H., An, O., Yang, H.H., Seshachalam, V.P., Koh, J.L.Y., Chan, W.-K., Ng, S.Y., Soh, B.S., (2022). Robust generation of human-chambered cardiac or-ganoids from pluripotent stem cells for improved modelling of cardiovascular diseases. Stem Cell Research & Therapy 13, 529. DOI: https://doi.org/10.1186/s13287-022-03215-1

Hockemeyer, D., Jaenisch, R., (2016). Induced Pluripotent Stem Cells Meet Genome Editing. Cell Stem Cell 18, 573–586. DOI: https://doi.org/10.1016/j.stem.2016.04.013

Horitani, K., Shiojima, I., (2024). Wnt signaling in cardiac development and heart diseases. In Vitro Cellular & Developmental Biology - Animal 60, 482–488. DOI: https://doi.org/10.1007/s11626-024-00917-z

Häkli, M., Jäntti, S., Joki, T., Sukki, L., Tornberg, K., Aalto-Setälä, K., Kallio, P., Pekkanen-Mattila, M., Narkilahti, S., (2022). Human Neurons Form Axon-Mediated Functional Connections with Human Cardiomyocytes in Compartmentalized Microfluidic Chip. International Journal of Mo-lecular Sciences 23, 3148. DOI: https://doi.org/10.3390/ijms23063148

Häkli, M., Kreutzer, J., Mäki, A.-J., Välimäki, H., Lappi, H., Huhtala, H., Kallio, P., Aalto-Setälä, K., Pekkanen-Mattila, M., (2021). Human induced pluripotent stem cell-based platform for modeling cardiac ischemia. Scientific Reports 11, 4153. DOI: https://doi.org/10.1038/s41598-021-83740-w

Idais, D., Roche, C.D., Kalogianni, G., Polonchuk, L., Gentile, C., (2025). Generation and applica-tions of cardiac spheroids. npj Biomedical Innovations 2, 17. DOI: https://doi.org/10.1038/s44385-025-00024-y

Jääskeläinen, P., Vangipurapu, J., Raivo, J., Kuulasmaa, T., Heliö, T., Aalto-Setälä, K., Kaartinen, M., Ilveskoski, E., Vanninen, S., Hämäläinen, L., Melin, J., Kokkonen, J., Nieminen, M.S., The FinHCM Study Group, Laakso, M., Kuusisto, J., (2019). Genetic basis and outcome in a na-tionwide study of Finnish patients with hypertrophic cardiomyopathy. ESC Heart Failure 6, 436–445. DOI: https://doi.org/10.1002/ehf2.12420

Kolde, R., (2025). pheatmap. DOI: https://doi.org/10.32614/CRAN.package.pheatmap

Landstrom, A.P., Kellen, C.A., Dixit, S.S., Van Oort, R.J., Garbino, A., Weisleder, N., Ma, J., Wehrens, X.H.T., Ackerman, M.J., (2011). Junctophilin-2 Expression Silencing Causes Cardi-ocyte Hypertrophy and Abnormal Intracellular Calcium-Handling. Circulation: Heart Failure 4, 214–223. DOI: https://doi.org/10.1161/CIRCHEARTFAILURE.110.958694

Lee, S.-G., Kim, Y.-J., Son, M.-Y., Oh, M.-S., Kim, J., Ryu, B., Kang, K.-R., Baek, J., Chung, G., Woo, D.H., Kim, C.-Y., Chung, H.M., (2022). Generation of human iPSCs derived heart or-ganoids structurally and functionally similar to heart. Biomaterials 290, 121860. DOI: https://doi.org/10.1016/j.biomaterials.2022.121860

Lewis-Israeli, Y.R., Wasserman, A.H., Gabalski, M.A., Volmert, B.D., Ming, Y., Ball, K.A., Yang, W., Zou, J., Ni, G., Pajares, N., Chatzistavrou, X., Li, W., Zhou, C., Aguirre, A., (2021). Self-assembling human heart organoids for the modeling of cardiac development and

congenital heart disease. Nature Communications 12, 5142. DOI: https://doi.org/10.1038/s41467-021-25329-5

Li, J., Feng, X., Wei, X., (2022). Modeling hypertrophic cardiomyopathy with human cardiomyocytes derived from induced pluripotent stem cells. Stem Cell Research & Therapy 13, 232. DOI: https://doi.org/10.1186/s13287-022-02905-0

Litviňuková, M., Talavera-López, C., Maatz, H., Reichart, D., Worth, C.L., Lindberg, E.L., Kanda, M., Polanski, K., Heinig, M., Lee, M., Nadelmann, E.R., Roberts, K., Tuck, L., Fasouli, E.S., DeLaughter, D.M., McDonough, B., Wakimoto, H., Gorham, J.M., Samari, S., Mahbubani, K.T., Saeb-Parsy, K., Patone, G., Boyle, J.J., Zhang, Hongbo, Zhang, Hao, Viveiros, A., Oudit, G.Y., Bayraktar, O.A., Seidman, J.G., Seidman, C.E., Noseda, M., Hubner, N., Teichmann, S.A., (2020). Cells of the adult human heart. Nature 588, 466–472. DOI: https://doi.org/10.1038/s41586-020-2797-4

Liu, B., Wang, S., Ma, H., Deng, Y., Du, J., Zhao, Y., Chen, Y., (2025). Heart-on-a-chip: a revolutionary organ-on-chip platform for cardiovascular disease modeling. Journal of Translati-onal Medicine 23, 132. DOI: https://doi.org/10.1186/s12967-024-05986-y

Machiraju, P., Greenway, S.C., (2019). Current methods for the maturation of induced pluripotent stem cell-derived cardiomyocytes. World Journal of Stem Cells 11, 33–43. DOI: https://doi.org/10.4252/wjsc.v11.i1.33

Marian, A.J., Braunwald, E., (2017). Hypertrophic Cardiomyopathy: Genetics, Pathogenesis, Clinical Manifestations, Diagnosis, and Therapy. Circulation Research 121, 749–770. DOI: https://doi.org/10.1161/CIRCRESAHA.117.311059

Maron, B.J., Maron, M.S., (2013). Hypertrophic cardiomyopathy. The Lancet 381, 242–255. DOI: https://doi.org/10.1016/S0140-6736(12)60397-3

Matsushita, Y., Furukawa, T., Kasanuki, H., Nishibatake, M., Kurihara, Y., Ikeda, A., Kamatani, N., Takeshima, H., Matsuoka, R., (2007). Mutation of junctophilin type 2 associated with hyper-trophic cardiomyopathy. Journal of Human Genetics 52, 543–548. DOI: https://doi.org/10.1007/s10038-007-0149-y

Moilanen, J., Perola, M., Pöyhönen, M., Ripatti-Toledo, T., Aittomäki, K., (2025). Lääketieteellinen genetiikka (2. uudistettu painos). Kustannus Oy Duodecim.

Mosqueira, D., Smith, J.G.W., Bhagwan, J.R., Denning, C., (2019). Modeling Hypertrophic Cardiomyopathy: Mechanistic Insights and Pharmacological Intervention. Trends in Molecular Medicine 25, 775–790. DOI: https://doi.org/10.1016/j.molmed.2019.06.005

Ojala, M., Prajapati, C., Pölönen, R.-P., Rajala, K., Pekkanen-Mattila, M., Rasku, J., Larsson, K., Aalto-Setälä, K., (2016). Mutation-Specific Phenotypes in hiPSC-Derived Cardiomyocytes Car-rying Either Myosin-Binding Protein C Or α -Tropomyosin Mutation for Hypertrophic Cardi-omyopathy. Stem Cells International 1, 1684792. DOI: https://doi.org/10.1155/2016/1684792

Padala, S.K., Cabrera, J-A., Ellenbogen, K.A., (2020). Anatomy of the cardiac conduction system. Pacing and Clinical Electrophysiology 44, 15-25. DOI: https://doi.org/10.1111/pace.14107

Park, H.-J., De Jesus Morales, K.J., Bheri, S., Kassouf, B.P., Davis, M.E., (2021). Bidirectional Relationship Between Cardiac Extracellular Matrix and Cardiac Cells in Ischemic Heart Disease. Stem Cells 39, 1650–1659. DOI: https://doi.org/10.1002/stem.3445

Pawlina, W., (2024). Histology: a text and atlas with correlated cell and molecular biology (Ninth edition). Wolters Kluwer.

Poliwoda, S., Noor, N., Downs, E., Schaaf, A., Cantwell, A., Ganti, L., Kaye, A.D., Mosel, L.I., Carroll, C.B., Viswanath, O., Urits, I., (2022). Stem cells: a comprehensive review of origins and emerging clinical roles in medical practice. Orthopedic Reviews 14. DOI: https://doi.org/10.52965/001c.37498

Sala, L., Van Meer, B.J., Tertoolen, L.G.J., Bakkers, J., Bellin, M., Davis, R.P., Denning, C., Dieben, M.A.E., Eschenhagen, T., Giacomelli, E., Grandela, C., Hansen, A., Holman, E.R., Jongbloed, M.R.M., Kamel, S.M., Koopman, C.D., Lachaud, Q., Mannhardt, I., Mol, M.P.H., Mosqueira, D., Orlova, V.V., Passier, R., Ribeiro, M.C., Saleem, U., Smith, G.L., Burton, F.L., Mummery, C.L., (2018). MUSCLEMOTION: A Versatile Open Software Tool to Quantify Cardiomyocyte and Cardiac Muscle Contraction In Vitro and In Vivo. Circulation Research 122. DOI: https://doi.org/10.1161/CIRCRESAHA.117.312067

Samak, M., Fatullayev, J., Sabashnikov, A., Zeriouh, M., Schmack, B., Farag, M., Popov, A.-F., Dohmen, P.M., Choi, Y.-H., Wahlers, T., Weymann, A., (2016). Cardiac Hypertrophy: An

Introduction to Molecular and Cellular Basis. Medical Science Monitor Basic Research 22, 75–79. DOI: https://doi.org/10.12659/MSMBR.900437

Schlittler, M., Pramstaller, P.P., Rossini, A., De Bortoli, M., (2023). Myocardial Fibrosis in Hypertrophic Cardiomyopathy: A Perspective from Fibroblasts. International Journal of Molec-ular Sciences 24, 14845. DOI: https://doi.org/10.3390/ijms241914845

Shah, A., Seydafkan, S., Sheps, D., (2022). Introduction to Cardiac Anatomy, Physiology, and Pathophysiology. Handbook of Cardiovascular Behavioral Medicine. Springer. DOI: https://doi.org/10.1007/978-0-387-85960-6

Takahashi, K., Tanabe, K., Ohnuki, M., Narita, M., Ichisaka, T., Tomoda, K., Yamanaka, S., (2007). Induction of Pluripotent Stem Cells from Adult Human Fibroblasts by Defined Factors. Cell 131, 861–872. DOI: https://doi.org/10.1016/j.cell.2007.11.019

Takahashi, K., Yamanaka, S., (2006). Induction of Pluripotent Stem Cells from Mouse Embryonic and Adult Fibroblast Cultures by Defined Factors. Cell 126, 663–676. DOI: https://doi.org/10.1016/j.cell.2006.07.024

Tian, Y., Cohen, E.D., Morrisey, E.E., (2010). The Importance of Wnt Signaling in Cardiovascular Development. Pediatric Cardiololy 31, 342–348. DOI: https://doi.org/10.1007/s00246-009-9606-z

Tian, Z., Yu, T., Wang, T., Higuchi, A., (2023). Introduction to stem cells. Progress in Molecular Biology and Translational Science 199, 3-32. DOI: 10.1016/bs.pmbts.2023.02.012

Tzec-Interián, J.A., González-Padilla, D., Góngora-Castillo, E.B., (2025). Bioinformatics perspecti-ves on transcriptomics: A comprehensive review of bulk and single-cell RNA sequencing ana-lyses. Quantitative Biology 13. DOI: https://doi.org/10.1002/qub2.78

Valtonen, J., Prajapati, C., Cherian, R.M., Vanninen, S., Ojala, M., Leivo, K., Heliö, T., Koskenvuo, J., Aalto-Setälä, K., (2023). The Junctophilin-2 Mutation p.(Thr161Lys) Is Associated with Hypertrophic Cardiomyopathy Using Patient-Specific iPS Cardiomyocytes and Demonstrates Prolonged Action Potential and Increased Arrhythmogenicity. Biomedicines 11, 1558. DOI: https://doi.org/10.3390/biomedicines11061558

Van Den Dolder, F.W., Dinani, R., Warnaar, V.A.J., Vučković, S., Passadouro, A.S., Nassar, A.A., Ramsaroep, A.X., Burchell, G.B., Schoonmade, L.J., Van Der Velden, J., Goversen, B.,

(2025). Experimental Models of Hypertrophic Cardiomyopathy. JACC: Basic to Translational Science 10, 511–546. DOI: https://doi.org/10.1016/j.jacbts.2024.10.017

van Meer, B.J., Sala L., Tertoolen, L.G.J., Smith, G.L., Burton, F.L., Mummery, C.L., (2018). Quantification of Muscle Contraction In Vitro and In Vivo Using MUSCLEMOTION Soft-ware: From Stem Cell-Derived Cardiomyocytes to Zebrafish and Human Hearts. Current Proto-cols in Human Genetics, 99. DOI: 10.1002/cphg.67

Vanninen, S.U.M., Leivo, K., Seppälä, E.H., Aalto-Setälä, K., Pitkänen, O., Suursalmi, P., Annala, A.-P., Anttila, I., Alastalo, T.-P., Myllykangas, S., Heliö, T.M., Koskenvuo, J.W., (2018). Het-erozygous junctophilin-2 (JPH2) p.(Thr161Lys) is a monogenic cause for HCM with heart fail-ure. PLOS ONE 13. DOI: https://doi.org/10.1371/journal.pone.0203422

Wickham, H., (2025). stringr. DOI: https://doi.org/10.32614/CRAN.package.stringr

Wickham, H., (2023). tidyverse. DOI: https://doi.org/10.32614/CRAN.package.tidyverse

Wickham, H., Bryan, J., Kalicinski, M., Valery, K., Leitienne, C., Colbert, B., Hoerl, D., Miller, E., (2026). readxl. DOI: https://doi.org/10.32614/CRAN.package.readxl

Wickham, H., François, R., Henry, L., Kirill, M., Vaughan, D., (2026). dplyr. DOI: https://doi.org/10.32614/CRAN.package.dplyr

Wickham, H., Chang, W., Henry, L., Pedersen, T.L., Takahashi, K., Wilke, C., Woo, K., Yutani, H., Dunnington, D., van den Brand, T., (2026). ggplot2. DOI: https://doi.org/10.32614/CRAN.package.ggplot2

Wickham, H., Vaughan, D., Girlich, M., Ushey, K., (2025). tidyr. DOI: https://doi.org/10.32614/CRAN.package.tidyr

Winer, J., Jung, C.K.S., Shackel, I., Williams, P.M., (1999). Development and Validation of Real-Time Quantitative Reverse Transcriptase–Polymerase Chain Reaction for Monitoring Gene Ex-pression in Cardiac Myocytesin Vitro. Analytical Biochemistry 270, 41–49. DOI: https://doi.org/10.1006/abio.1999.4085

Yamanaka, S., (2020). Pluripotent Stem Cell-Based Cell Therapy—Promise and Challenges. Cell Stem Cell 27, 523–531. DOI: https://doi.org/10.1016/j.stem.2020.09.014

Yamanaka, S., (2012). Induced Pluripotent Stem Cells: Past, Present, and Future. Cell Stem Cell 10, 678–684. DOI: https://doi.org/10.1016/j.stem.2012.05.005

Yang, H., Yang, Y., Kiskin, F.N., Shen, M., Zhang, J.Z., (2023). Recent advances in regulating the proliferation or maturation of human-induced pluripotent stem cell-derived cardiomyocytes. Stem Cell Research & Therapy 14, 228. DOI: https://doi.org/10.1186/s13287-023-03470-w

Yin, P.T., Han, E., Lee, K., (2016). Engineering Stem Cells for Biomedical Applications. Advanced Healthcare Materials 5, 10–55. DOI: https://doi.org/10.1002/adhm.201400842

Appendices

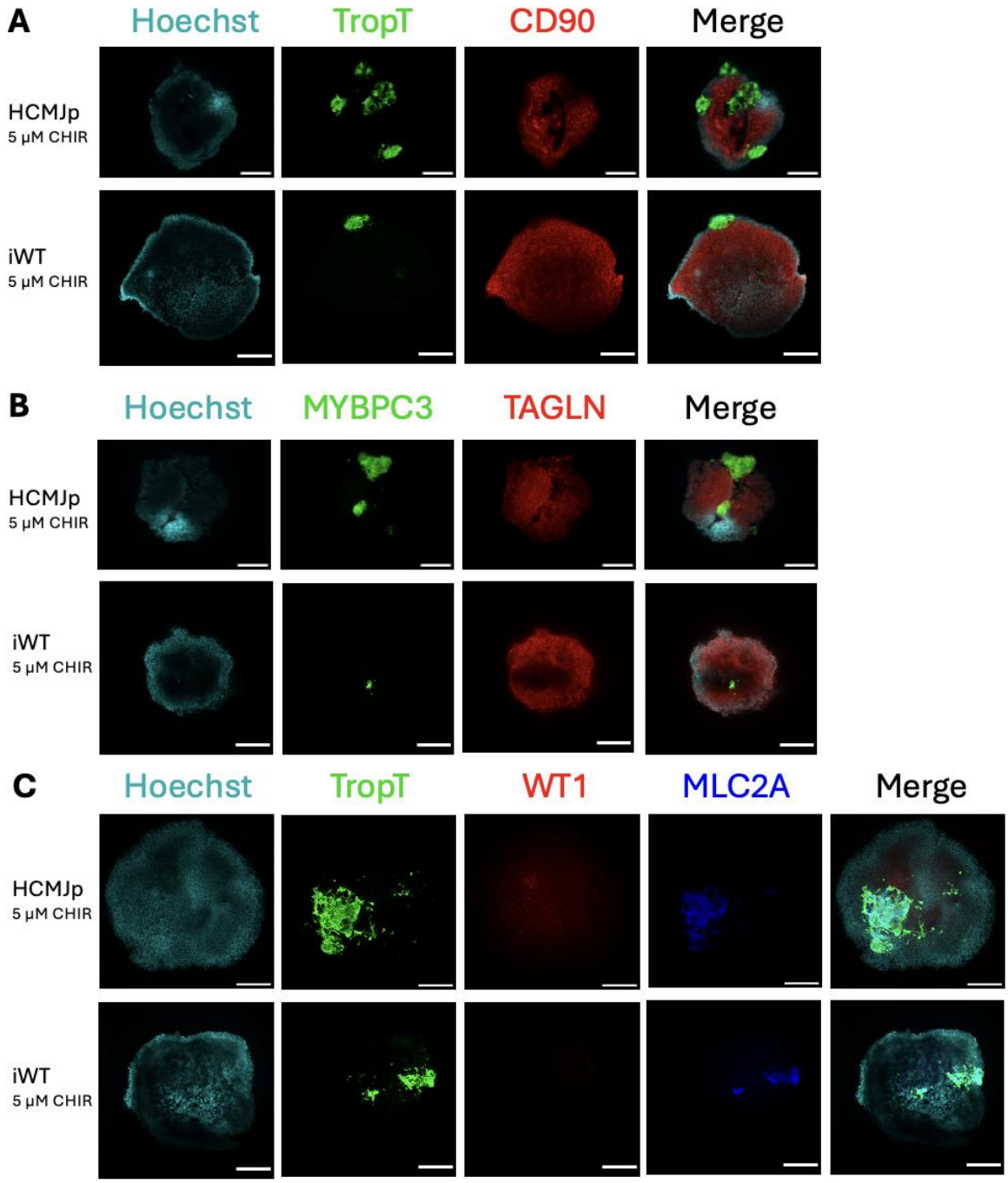

Supplementary figure 1. Heart organoids cultured in RPMI medium. Cellular composition was assessed using confocal immunofluorescence imaging at day 14 and day 28. **A:** Day 14 heart organoids stained for Hoechst (blue, nuclei), TropT (green, cardiomyocytes), and CD90 (red, fibroblasts). **B:** Day 14 heart organoids stained for Hoechst (blue), MYBPC3 (green, cardiomyocytes), and TAGLN (red, smooth muscle cells). **C:** Day 28 heart organoids stained for Hoechst (blue), TropT (green), WT1 (red, epicardial cells), and MLC2A (dark blue, atrial cardiomyocytes). Scale bar: 250 µm.